DETECTING GRAVITATIONAL WAVES

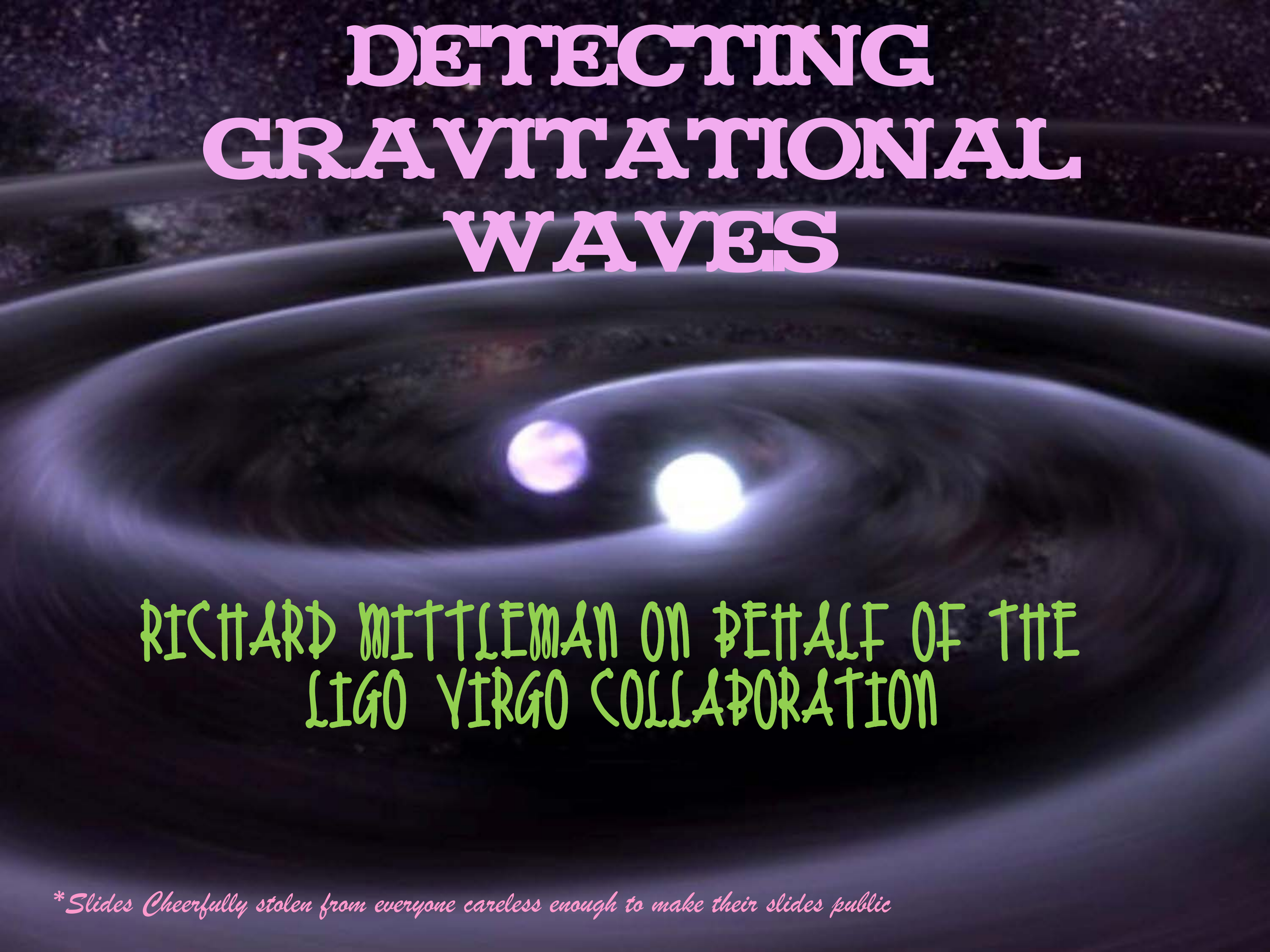

RICHARD MITTLEMAN ON BEHALF OF THE LIGO VIRGO COLLABORATION

**Slides Cheerfully stolen from everyone careless enough to make their slides public*

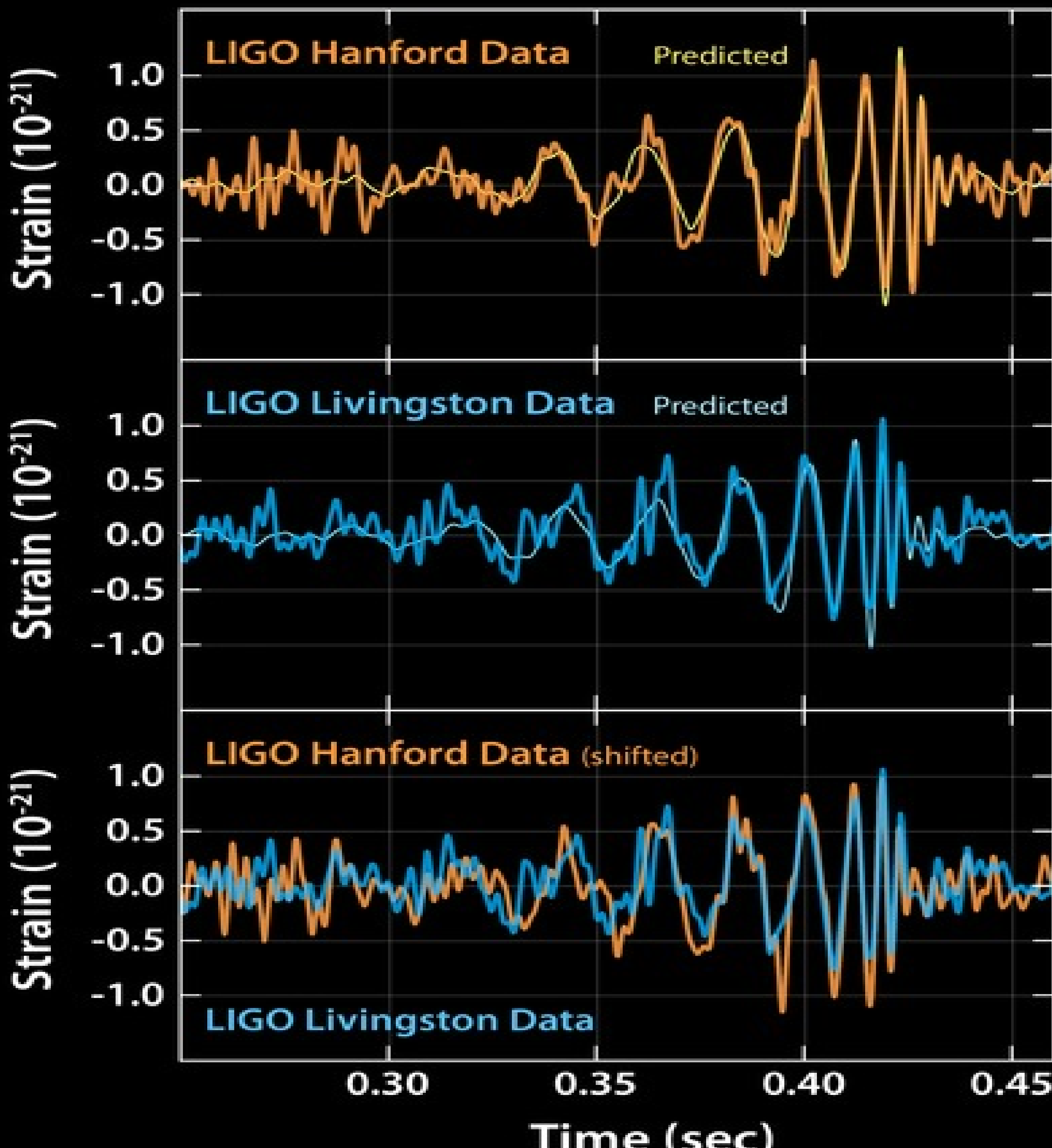
LIGO Hanford Data
Predicted
LIGO Livingston Data
Predicted
LIGO Hanford Data (shifted)
LIGO Livingston Data
Strain (10^{-21})
1.0
0.5
0.0
-0.5
-1.0
0.30
0.35
0.40
0.45
Time (sec)

a simulation of GW150914

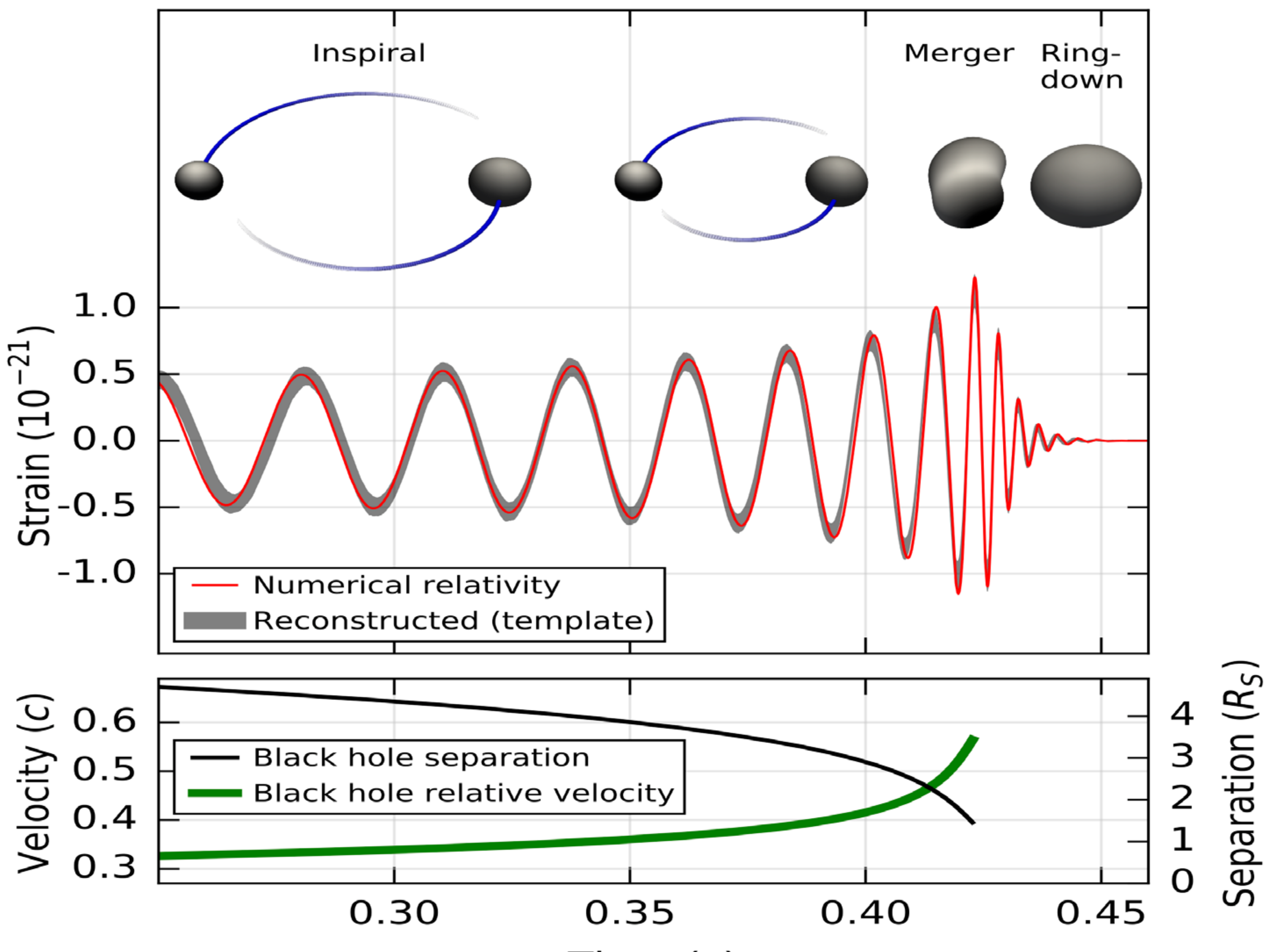

Inspiral
Merger
Ring-down
Strain (10^{-21})
1.0
0.5
0.0
-0.5
-1.0
Numerical relativity
Reconstructed (template)
Velocity (c)
0.6
0.5
0.4
0.3
Black hole separation
Black hole relative velocity
Separation (R_S)
4
3
2
1
0
0.30
0.35
0.40
0.45

Gravitational Waves in General Relativity (Einstein 1916,1918)

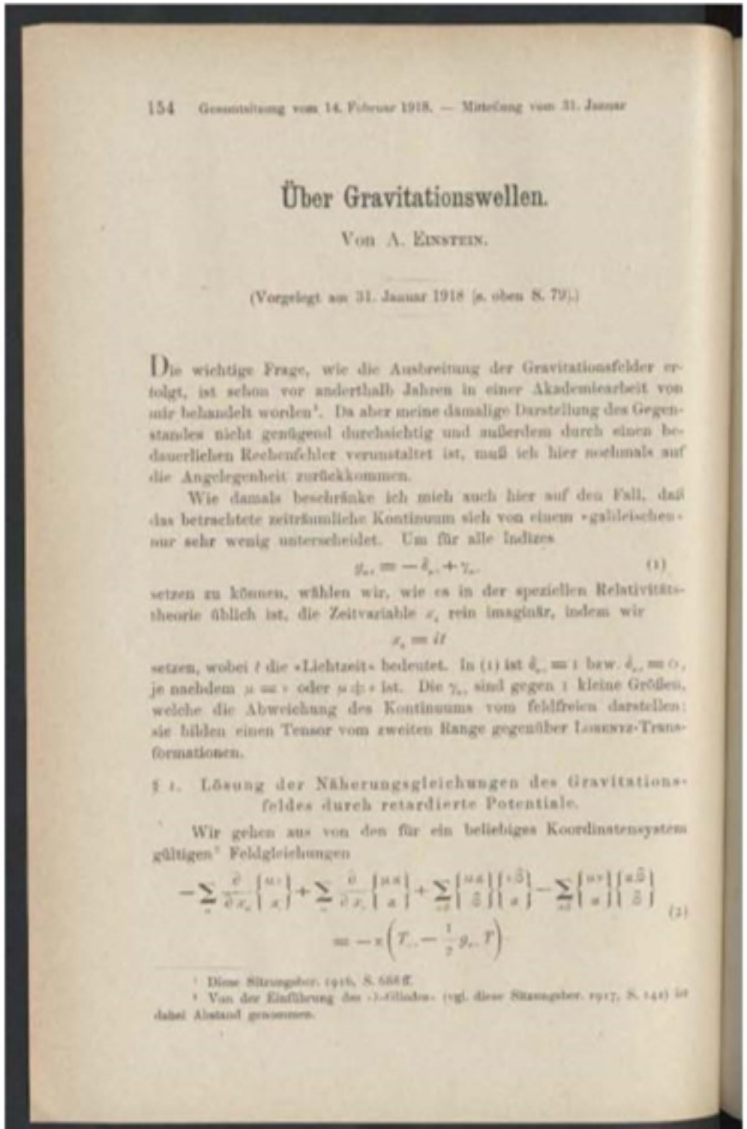

154 Gesamtsitzung vom 14. Februar 1918. — Mitteilung vom 31. Januar

Über Gravitationswellen.

Von A. Einstein.

(Vorgelegt am 31. Januar 1918 [s. oben S. 79].)

Die wichtige Frage, wie die Ausbreitung der Gravitationsfelder erfolgt, ist schon vor anderthalb Jahren in einer Akademiearbeit von mir behandelt worden[1]. Da aber meine damalige Darstellung des Gegenstandes nicht genügend durchsichtig und außerdem durch einen bedauerlichen Rechenfehler verunstaltet ist, muß ich hier nochmals auf die Angelegenheit zurückkommen.

Wie damals beschränke ich mich auch hier auf den Fall, daß das betrachtete zeiträumliche Kontinuum sich von einem »galileischen« nur sehr wenig unterscheidet. Um für alle Indizes

$$g_{\mu\nu} = -\delta_{\mu\nu} + \gamma_{\mu\nu} \qquad (1)$$

setzen zu können, wählen wir, wie es in der speziellen Relativitätstheorie üblich ist, die Zeitvariable x_4 rein imaginär, indem wir

$$x_4 = it$$

setzen, wobei t die »Lichtzeit« bedeutet. In (1) ist $\delta_{\mu\nu} = 1$ bzw. $\delta_{\mu\nu} = 0$, je nachdem $\mu = \nu$ oder $\mu \neq \nu$ ist. Die $\gamma_{\mu\nu}$ sind gegen 1 kleine Größen, welche die Abweichung des Kontinuums vom feldfreien darstellen; sie bilden einen Tensor vom zweiten Range gegenüber Lorentz-Transformationen.

§ 1. Lösung der Näherungsgleichungen des Gravitationsfeldes durch retardierte Potentiale.

Wir gehen aus von den für ein beliebiges Koordinatensystem gültigen[2] Feldgleichungen

$$-\sum_{\alpha}\frac{\partial}{\partial x_\alpha}\begin{Bmatrix}\mu\nu\\ \alpha\end{Bmatrix}+\sum_{\alpha}\frac{\partial}{\partial x_\nu}\begin{Bmatrix}\mu\alpha\\ \alpha\end{Bmatrix}+\sum_{\alpha\beta}\begin{Bmatrix}\mu\alpha\\ \beta\end{Bmatrix}\begin{Bmatrix}\nu\beta\\ \alpha\end{Bmatrix}-\sum_{\alpha\beta}\begin{Bmatrix}\mu\nu\\ \alpha\end{Bmatrix}\begin{Bmatrix}\alpha\beta\\ \beta\end{Bmatrix} = -\kappa\left(T_{\mu\nu}-\frac{1}{2}g_{\mu\nu}T\right) \qquad (2)$$

[1] Diese Sitzungsber. 1916, S. 688 ff.

[2] Von der Einführung des »λ-Gliedes« (vgl. diese Sitzungsber. 1917, S. 142) ist dabei Abstand genommen.

$$g_{ij} = \delta_{ij} + h_{ij}$$

h_{ij}: transverse, traceless and propagates at v=c

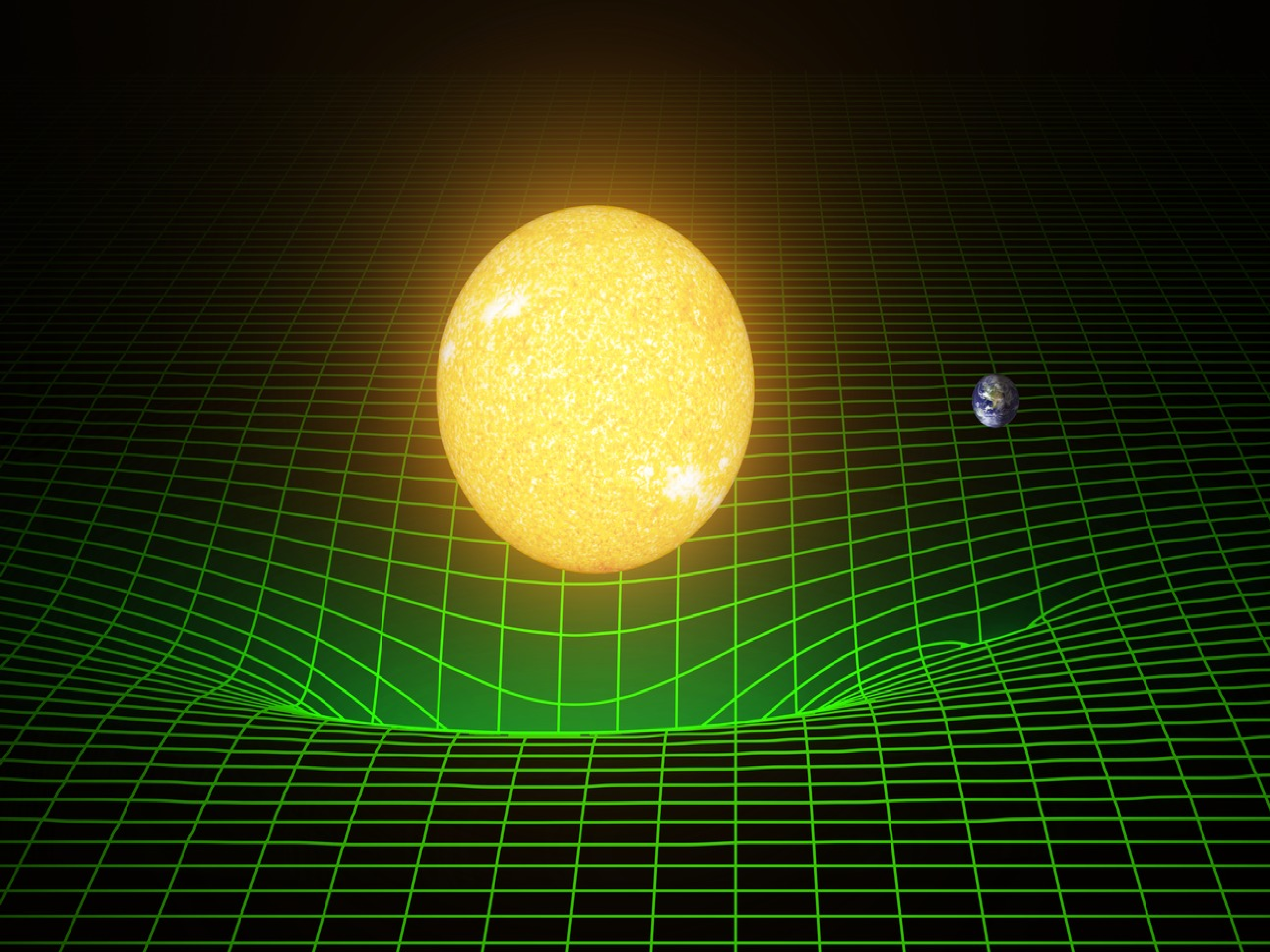

Radiation
is a Quadrupolar
Strain
in space-time

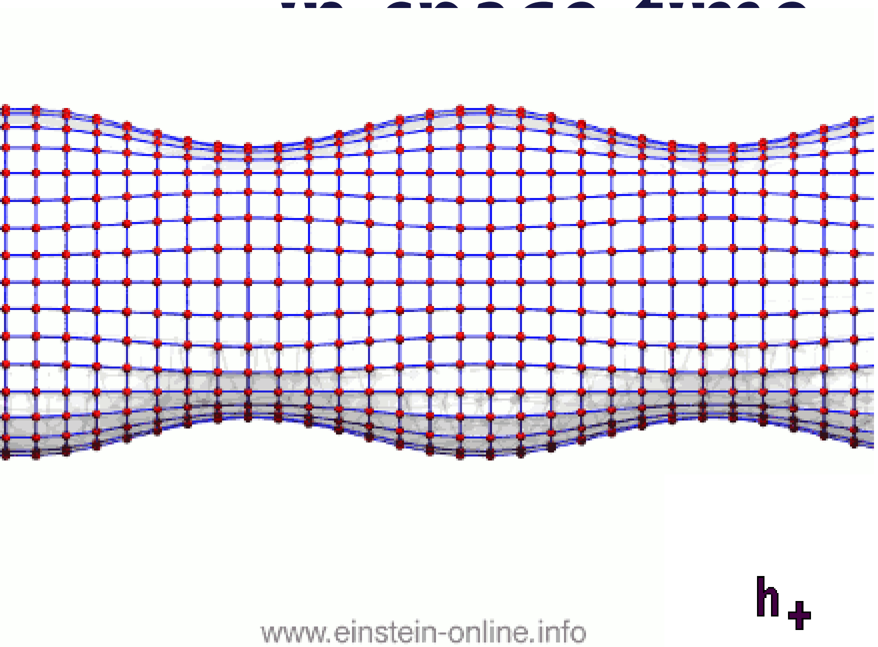

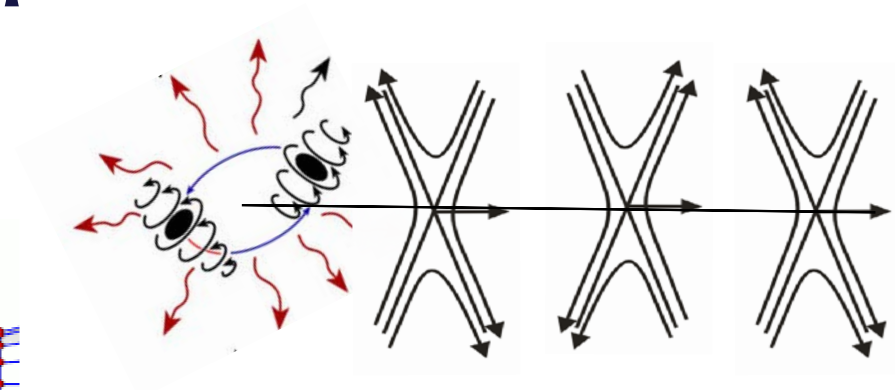

Space is very stiff
For astrophysical sources
you might expect h~1e-21

There are two polarizations

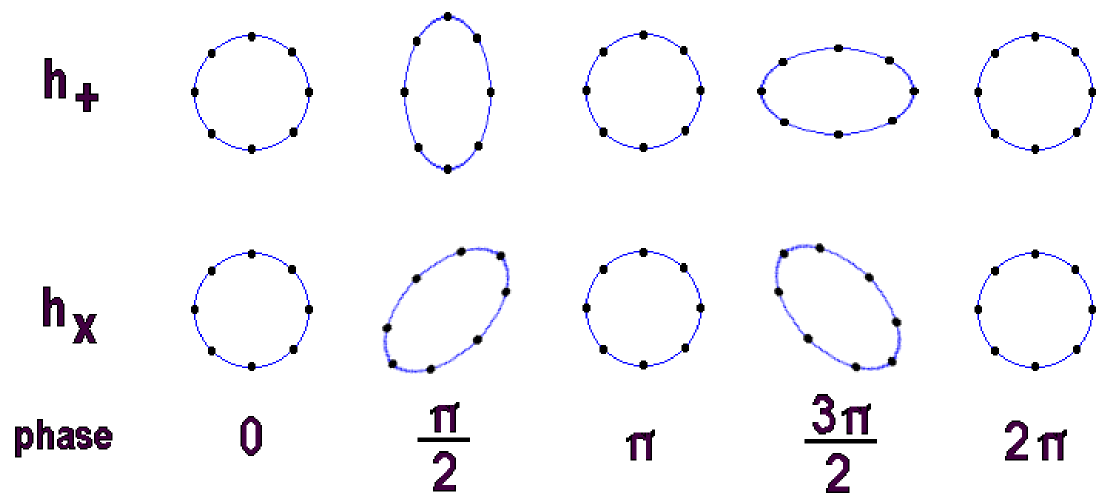

How big is the effect? Zooming into an Atom

Three(ish) Detections in the first science run (O1)

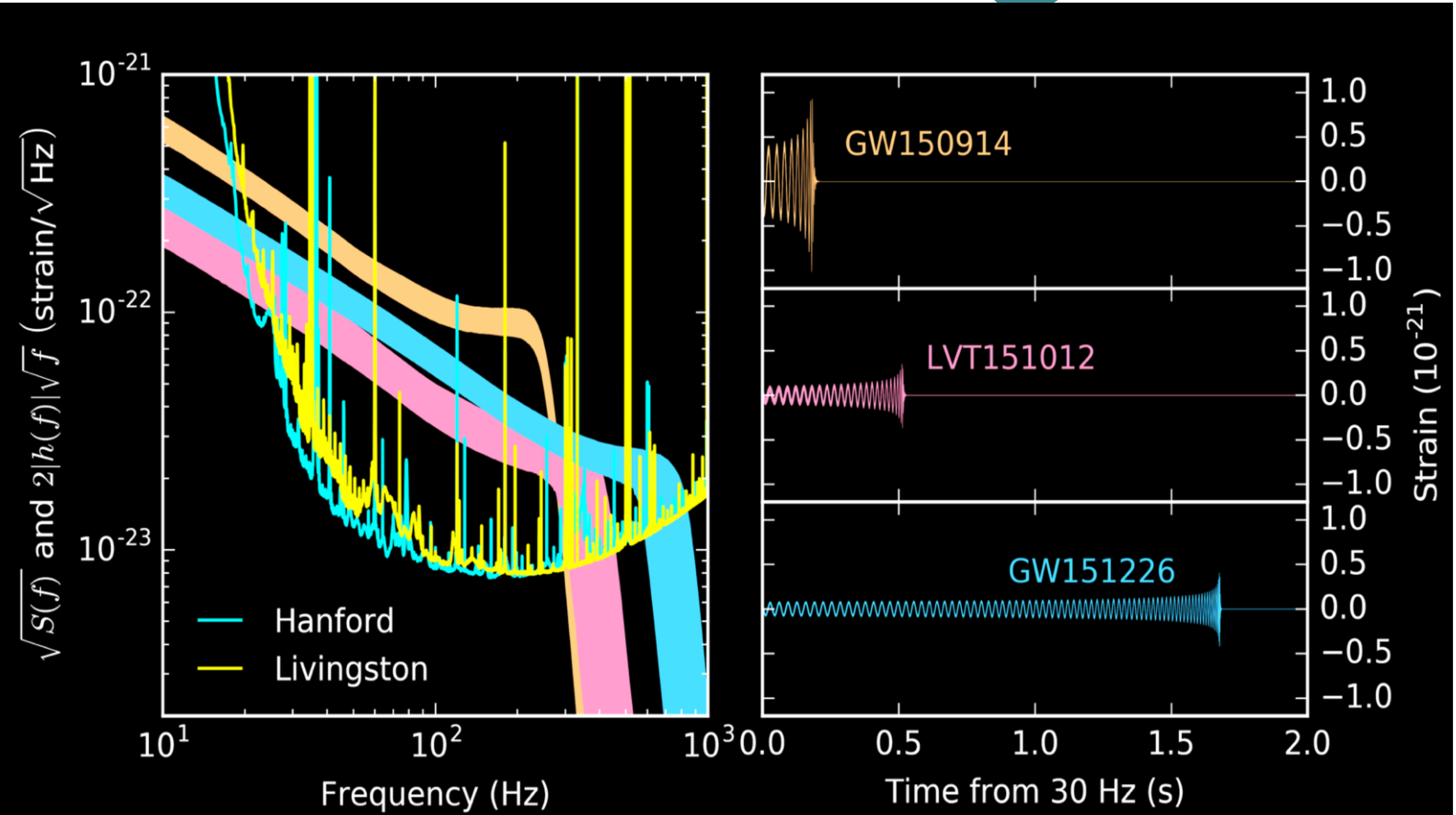

Abbott, ..., DAB, et al. arXix:1606.04856

LIGO Scientific Collaboration

- Australian Consortium for Interferometric Gravitational Astronom
- The Univ. of Adelaide
- Andrews University
- The Australian National Univ.
- The University of Birmingham
- California Inst. of Technology
- Cardiff University
- Carleton College
- Charles Stuart Univ.
- Columbia University
- Embry Riddle Aeronautical Univ.
- Eötvös Loránd University
- University of Florida
- German/British Collaboration for the Detection of Gravitational Waves
- University of Glasgow
- Goddard Space Flight Center
- Leibniz Universität Hannover
- Hobart & William Smith Colleges
- Inst. of Applied Physics of the Russian Academy of Sciences
- Polish Academy of Sciences
- India Inter-University Centre for Astronomy and Astrophysics
- Louisiana State University
- Louisiana Tech University
- Loyola University New Orleans
- University of Maryland
- Max Planck Institute for Gravit

- University of Michigan
- University of Minnesota
- The University of Mississippi
- Massachusetts Inst. of Technology
- Monash University
- Montana State University
- Moscow State University
- National Astronomical Observatory of Japan
- Northwestern University
- University of Oregon
- Pennsylvania State University
- Rochester Inst. of Technology
- Rutherford Appleton Lab
- University of Rochester
- San Jose State University
- Univ. of Sannio at Benevento, and Univ. of Salerno
- University of Sheffield
- University of Southampton
- Southeastern Louisiana Univ.
- Southern Univ. and A&M College
- Stanford University
- University of Strathclyde
- Syracuse University
- Univ. of Texas at Austin
- Univ. of Texas at Brownsville
- Trinity University
- Universitat de les Illes Balears
- Univ. of Massachusetts Amherst
- University of Western Australia
- Univ. of Wisconsin-Milwaukee
- Washington State University
- University of Washington

ART. XXXVI.—*On the Relative Motion of the Earth and the Luminiferous Ether*; by ALBERT A. MICHELSON and EDWARD W. MORLEY.*

American Journal of Science, Nov 1887 vol. Series 3 Vol. 34 no. 203 333-345

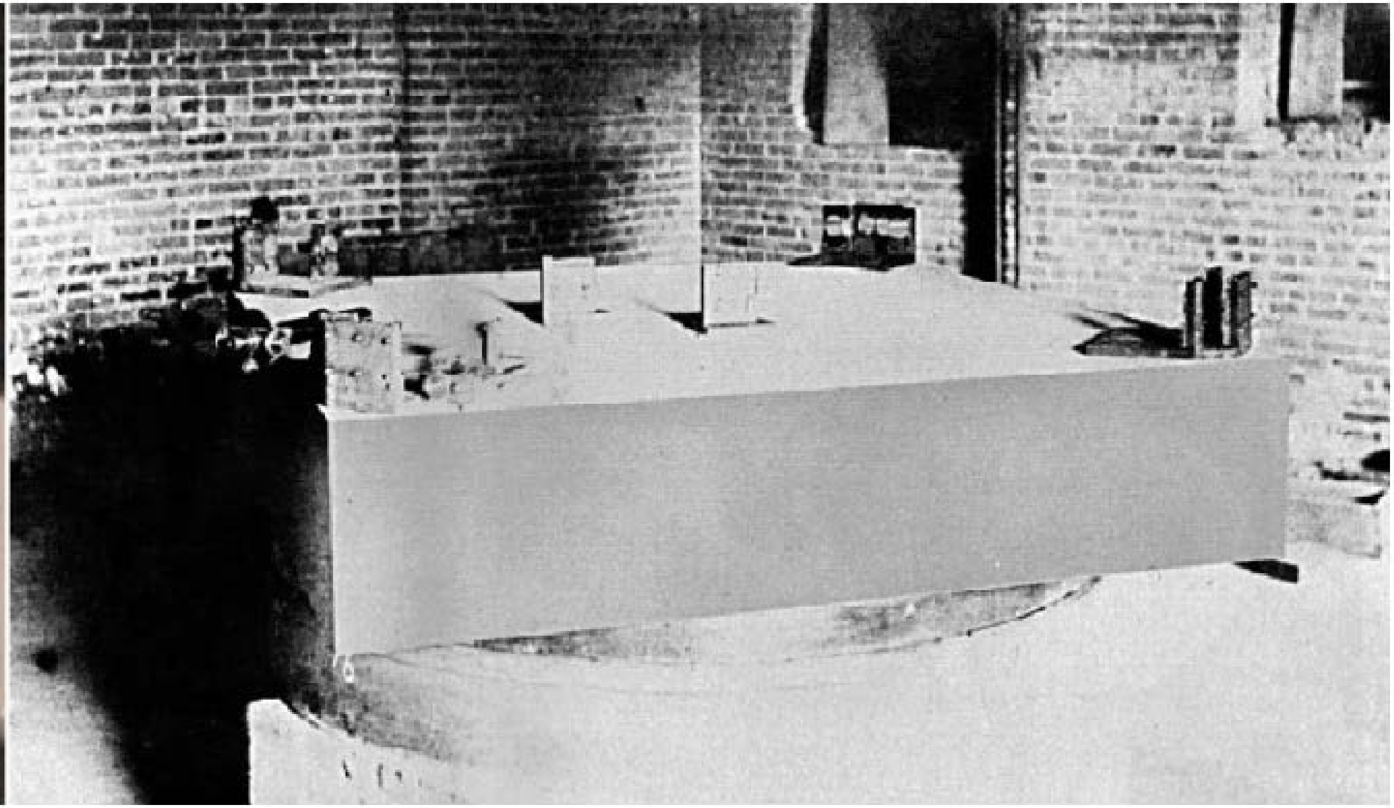

Used light interferometry to achieve sensitivity in measuring distances down to 0.01 λ or ~5×10^{-9} m = 0.000000005 m

1907 Nobel Prize in Physics to A. Michelson

Simple Michaelson Interferometer

ENHANCED LIGO

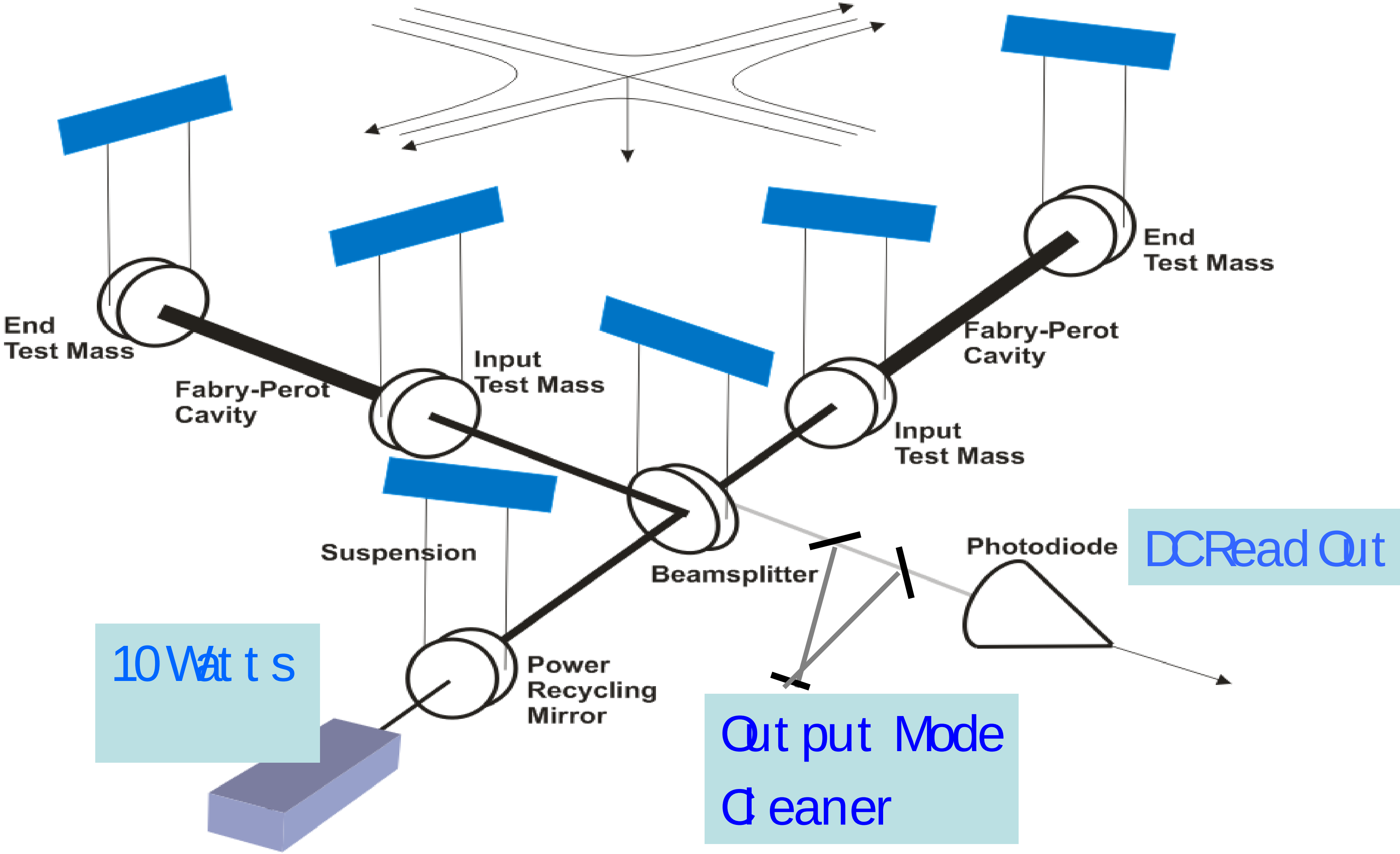

ADVANCED LIGO

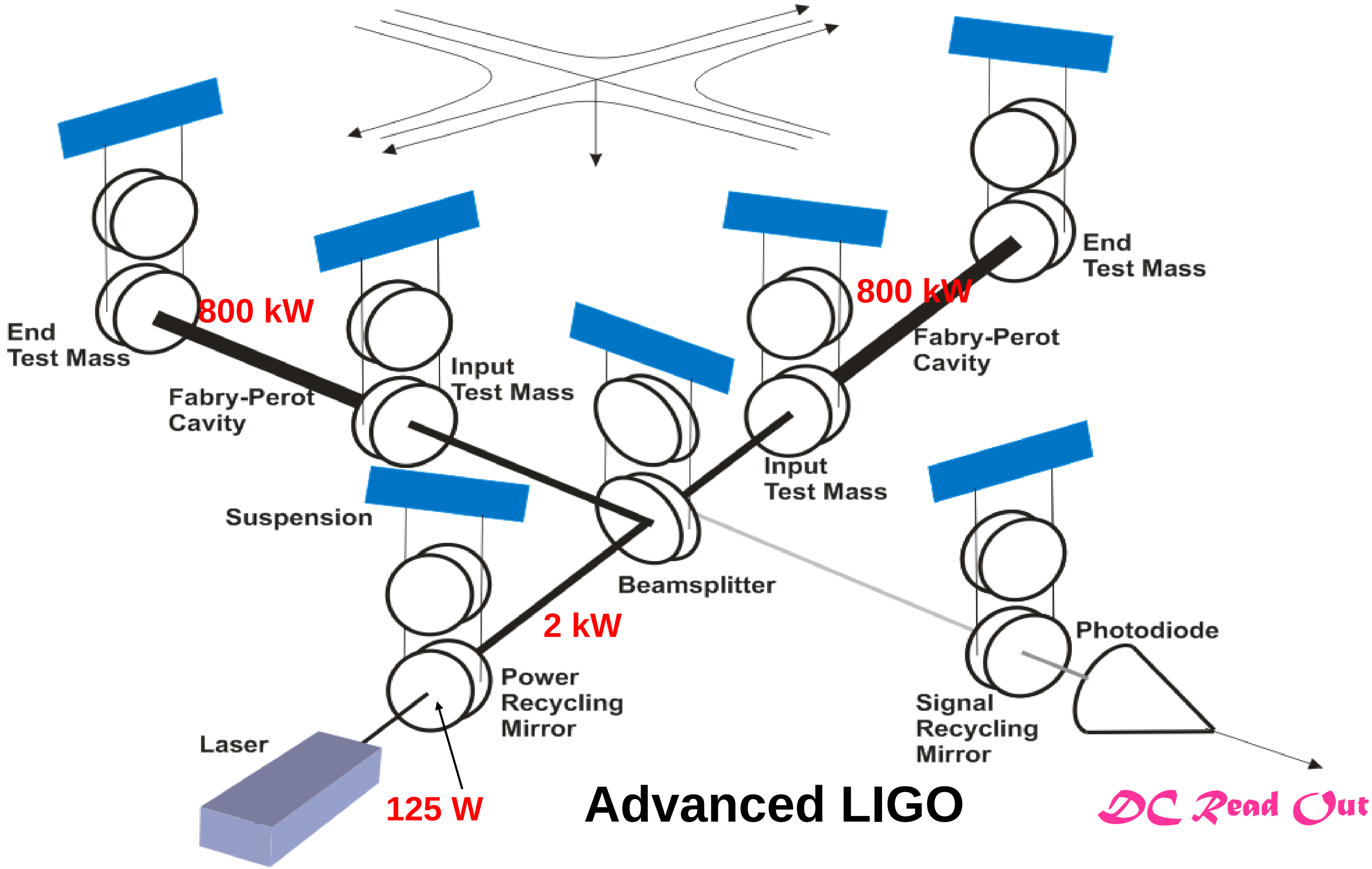

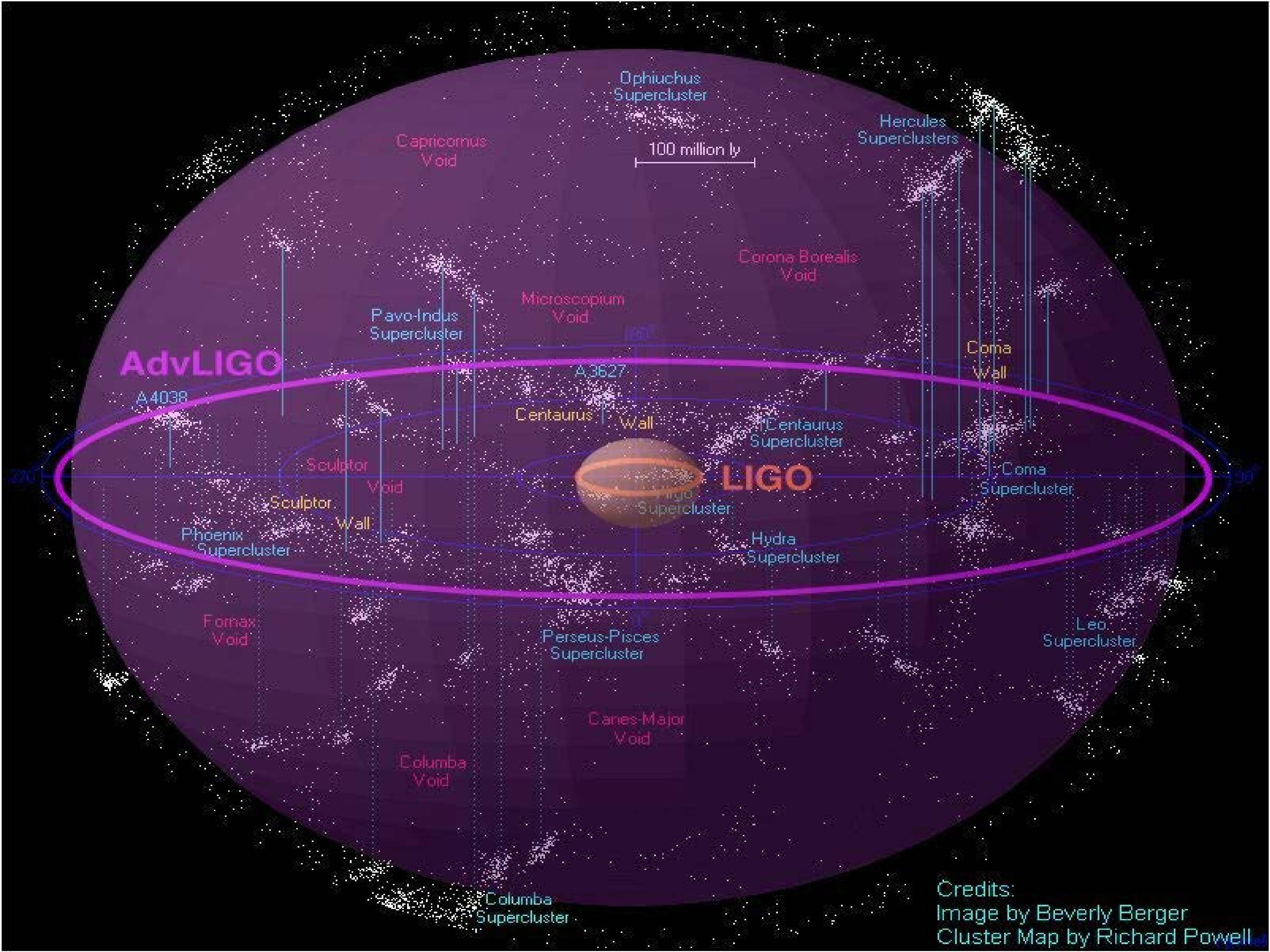
Ophiuchus Supercluster
Capricornus Void
100 million ly
Hercules Superclusters
Corona Borealis Void
Microscopium Void
Pavo-Indus Supercluster
Coma Wall
AdvLIGO
A3627
A4038
Centaurus Wall
Centaurus Supercluster
Sculptor Void
LIGO
Coma Supercluster
Sculptor Wall
Virgo Supercluster
Phoenix Supercluster
Hydra Supercluster
Fornax Void
Perseus-Pisces Supercluster
Leo Supercluster
Canes-Major Void
Columba Void
Columba Supercluster
Credits:
Image by Beverly Berger
Cluster Map by Richard Powell


~3000 km
Mar 4, 2010 8:25 pm
Mar 3, 2010
Mar 4, 2010
New York
Washington
United States
Pasadena
Livingston
Gulf of California
1475 km
© 2010 Europa Technologies
© 2010 Tele Atlas
Data SIO, NOAA, U.S. Navy, NGA, GEBCO
© 2010 Google
Gulf of Mexico
Nassau
The Bahamas
©2009 Google

LIGO

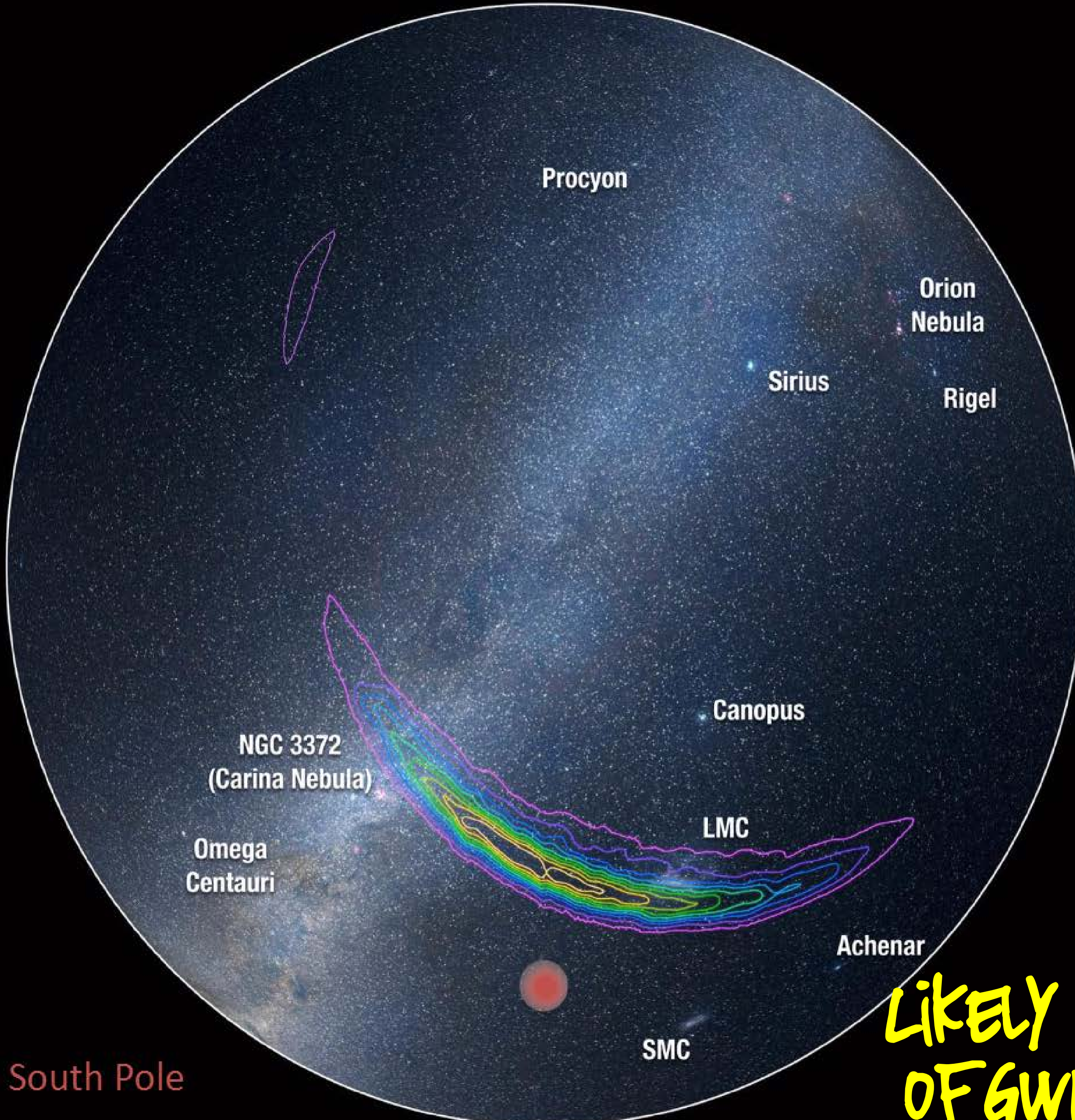

LIKELY LOCATIO
OF GW150914

South Pole

The Global Network of Gravitational Wave Detectors

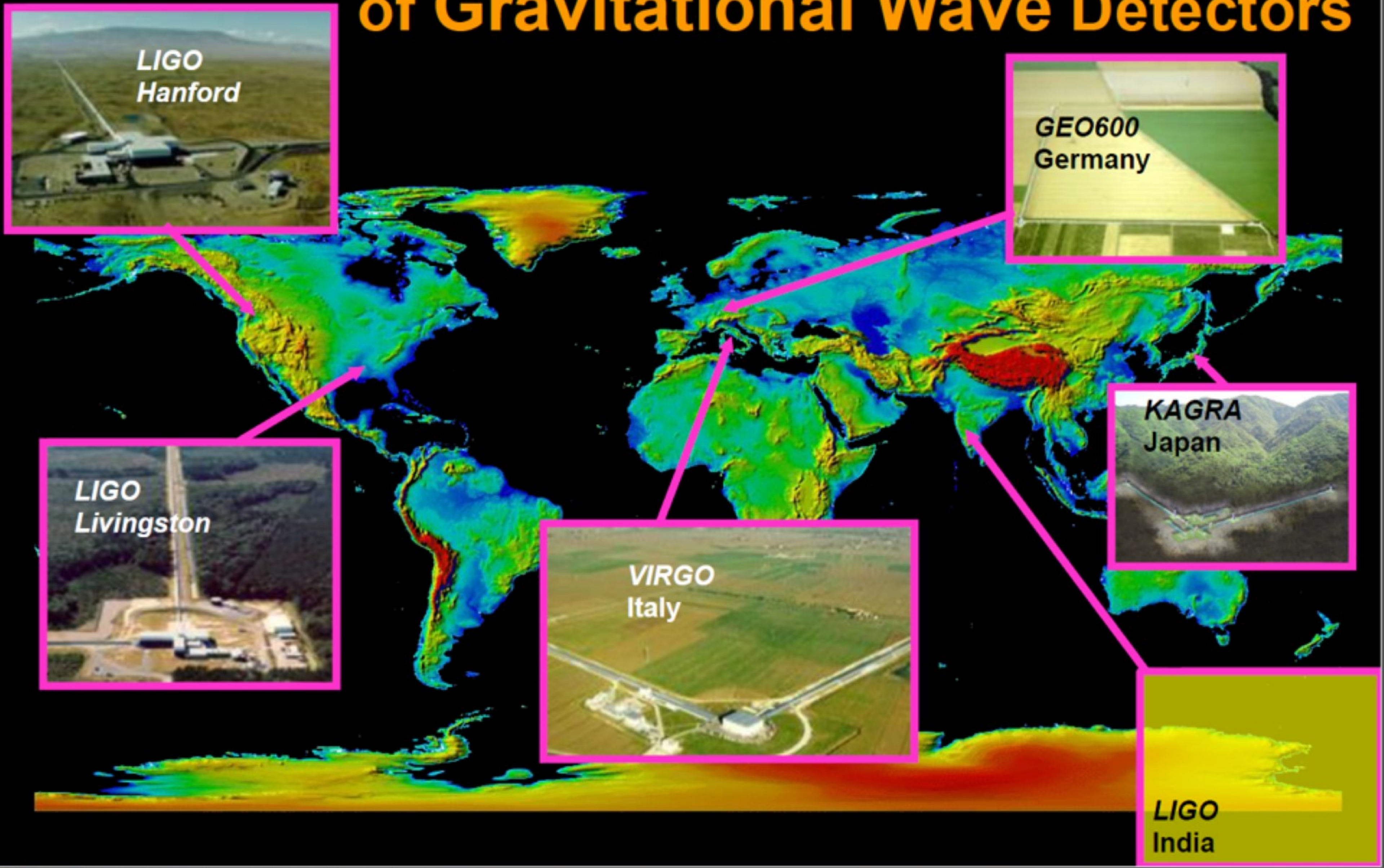

LIGO Livingston

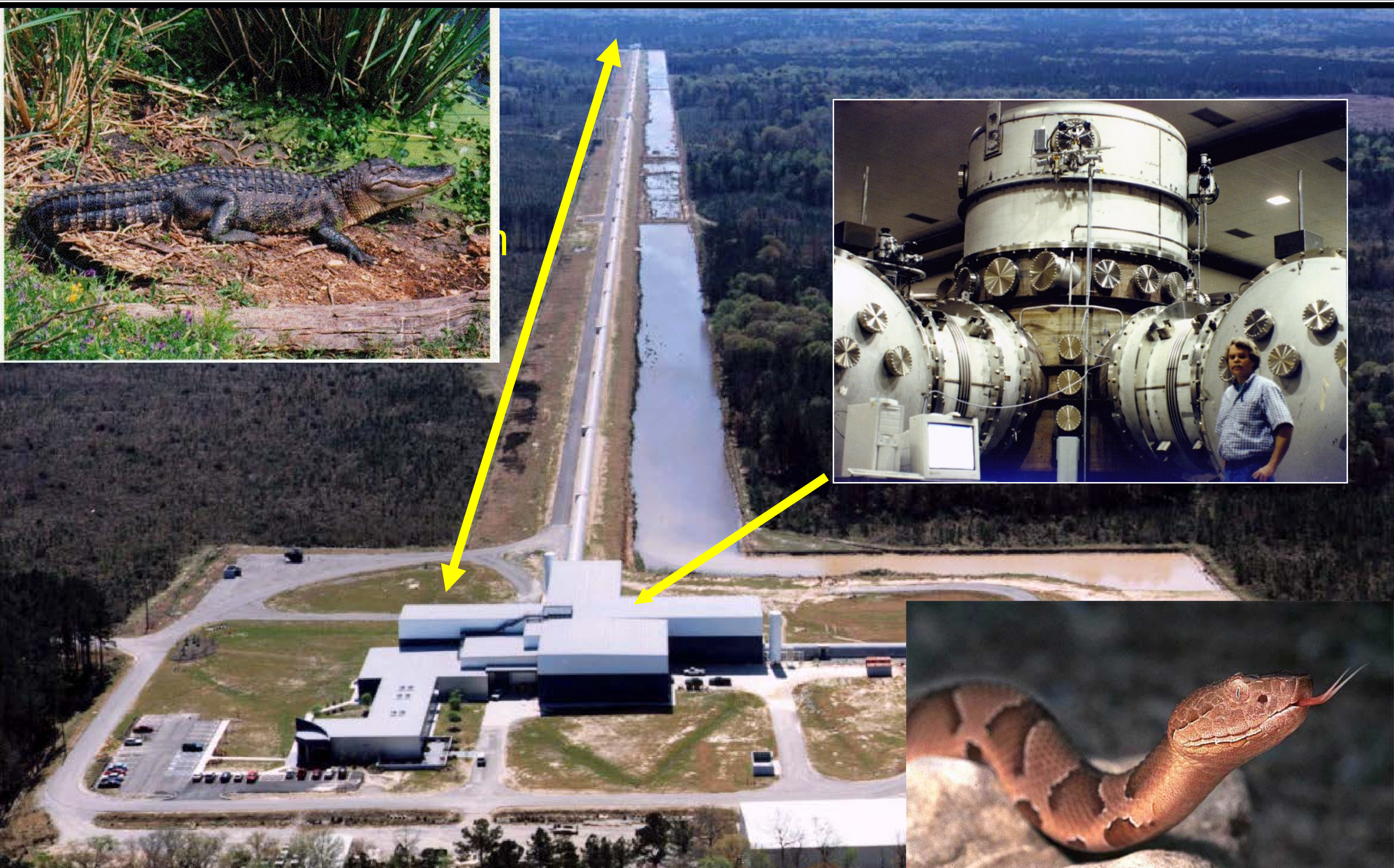

LIGO Hanford


VIRGO
CASCINA, ITALY

- Young (~300 yr) compact object
- Position is well known
- Unknown spin-down parameters

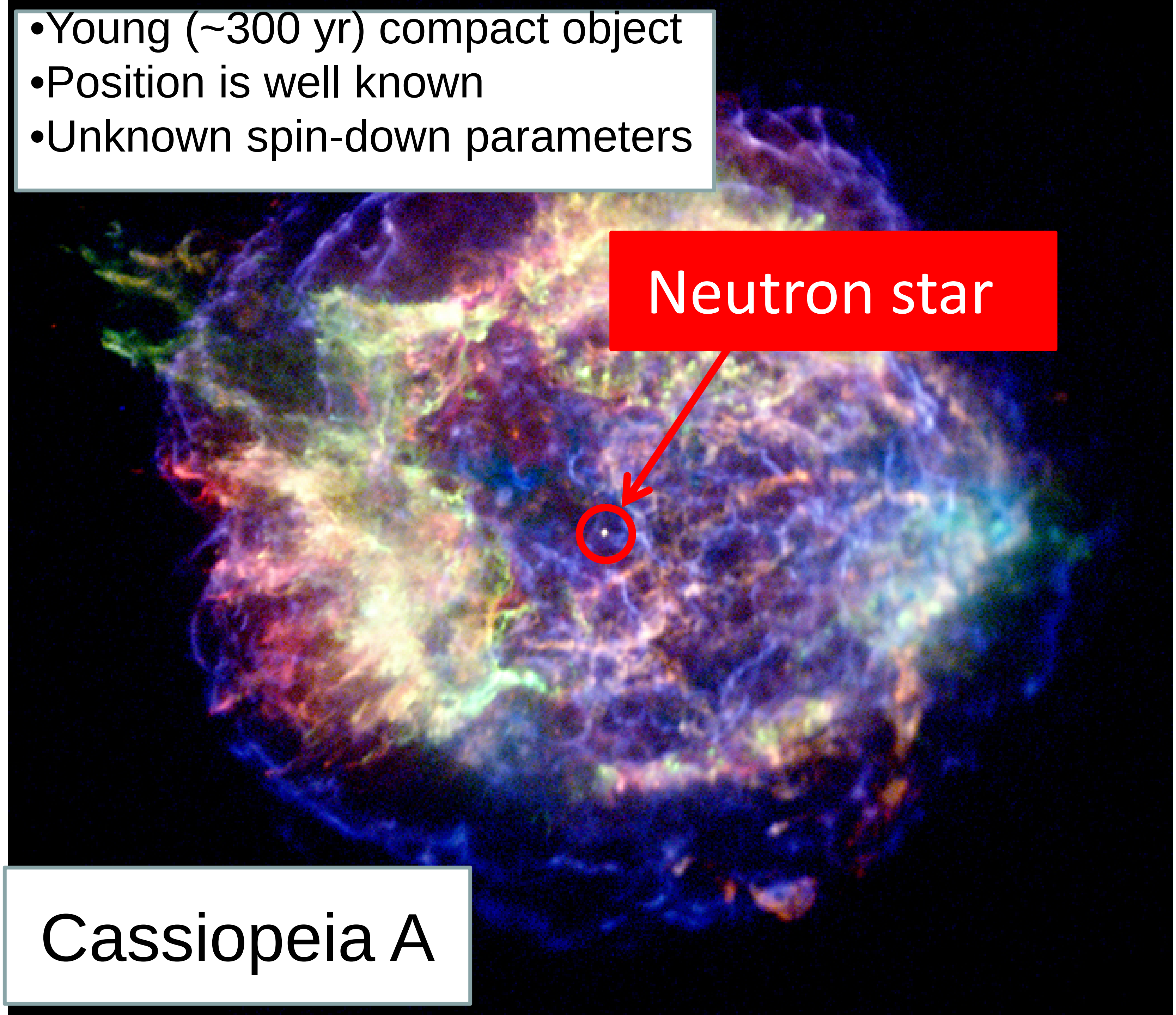

Cassiopeia A

Neutron Star Inspiral

The binary pulsar

- Period speeds up 14 sec from 1975-94
- Measured to ~50 msec accuracy
- Deviation grows quadratically with time
- Merger in about 300M years
  (<< age of universe!)
- shortening of period ⇐ orbital energy loss
- Compact system:
  negligible loss from friction, material flow
- Beautiful agreement with GR prediction
- Apparently, loss is due to GWs!
- GW emission will be strongest near the end:
  – Coalescence of neutron stars!
- Nobel Prize, 1993
- By 2013, there are ~8

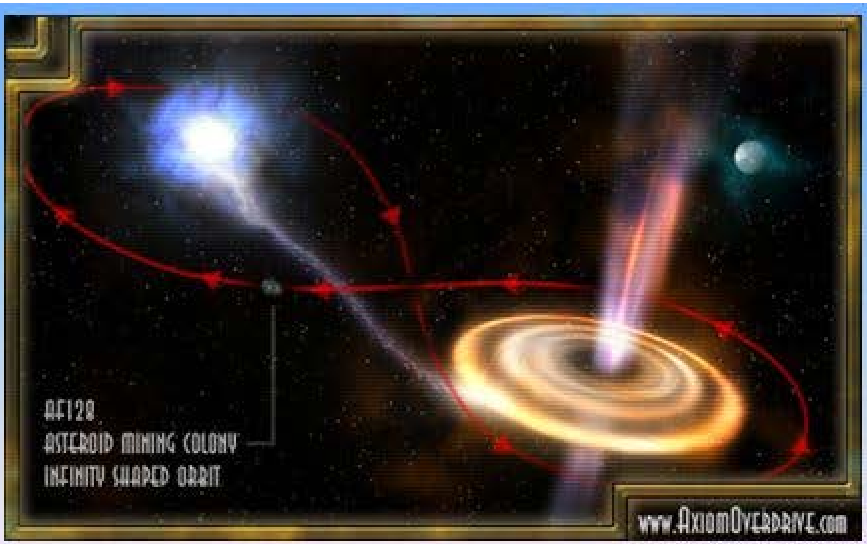

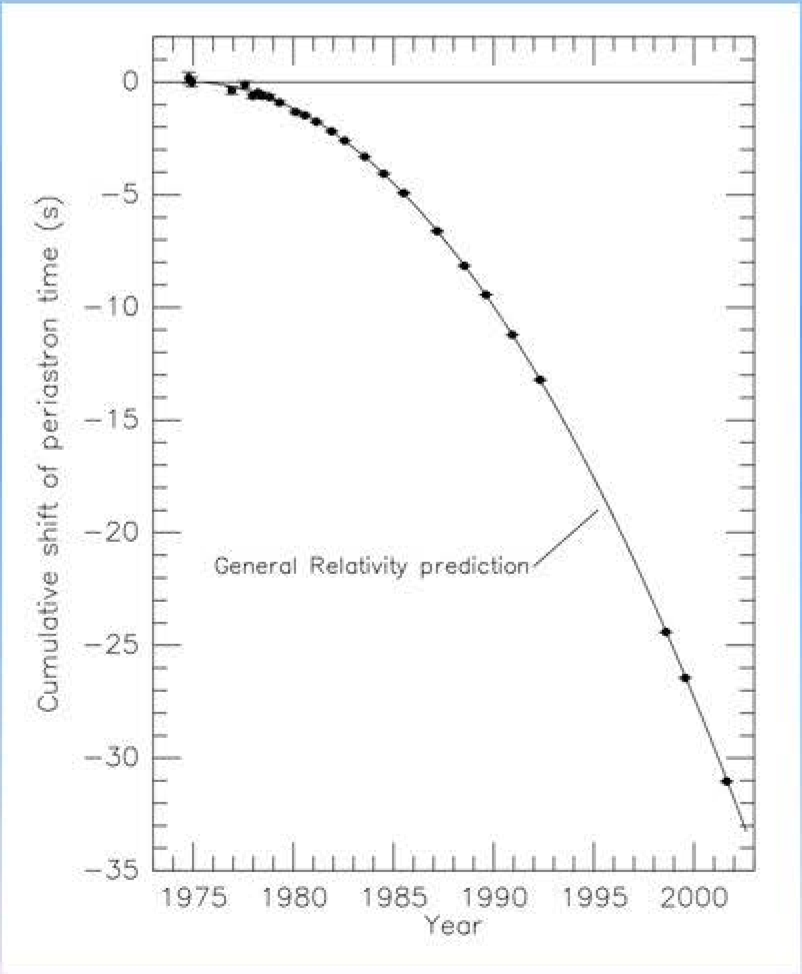

Stochastic background*

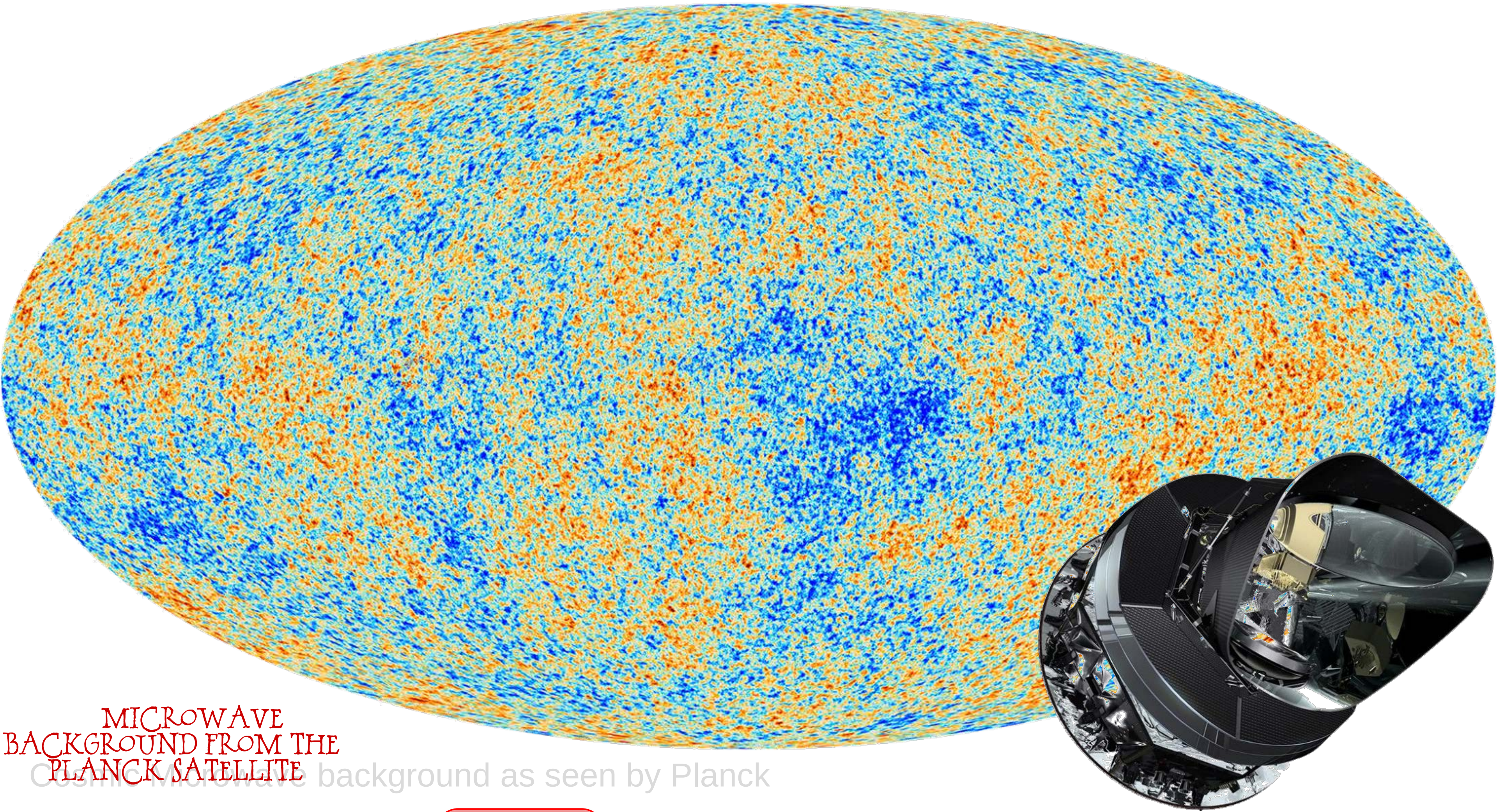

MICROWAVE BACKGROUND FROM THE PLANCK SATELLITE

Cosmic Microwave background as seen by Planck

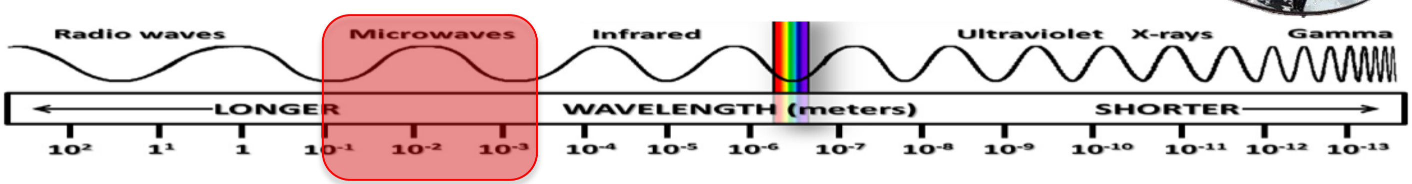

The GW Spectrum

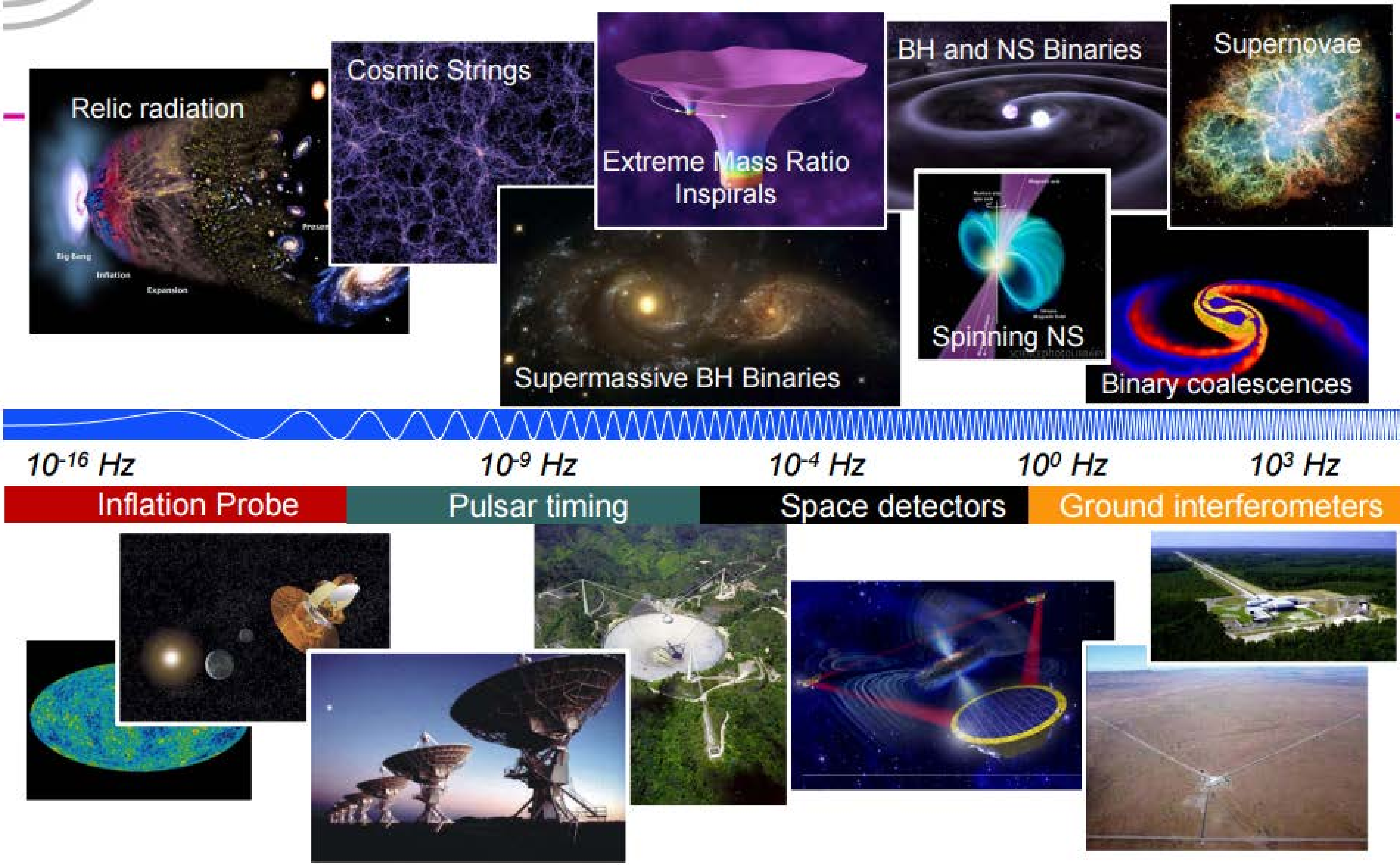

Noise Cartoon

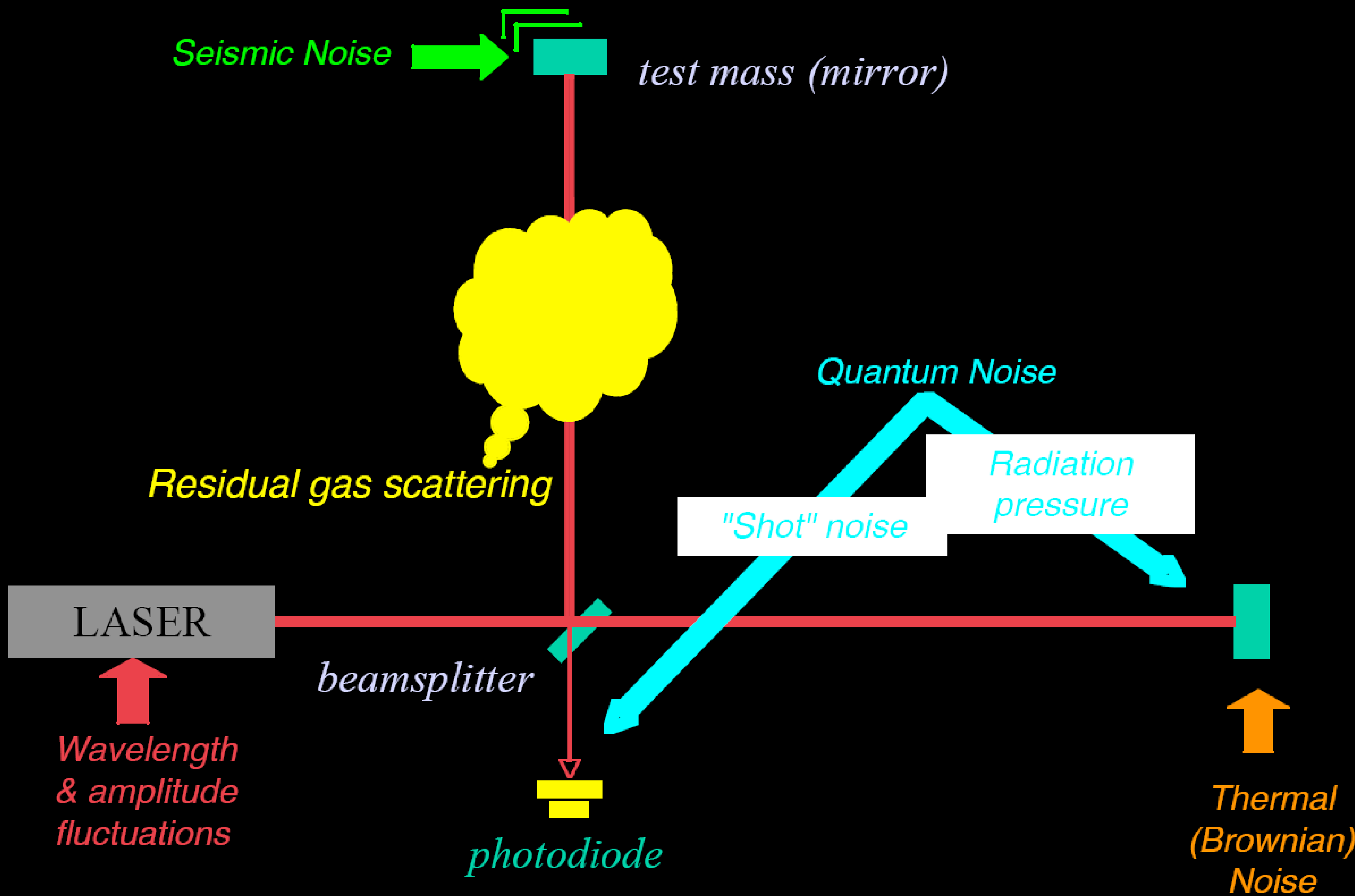

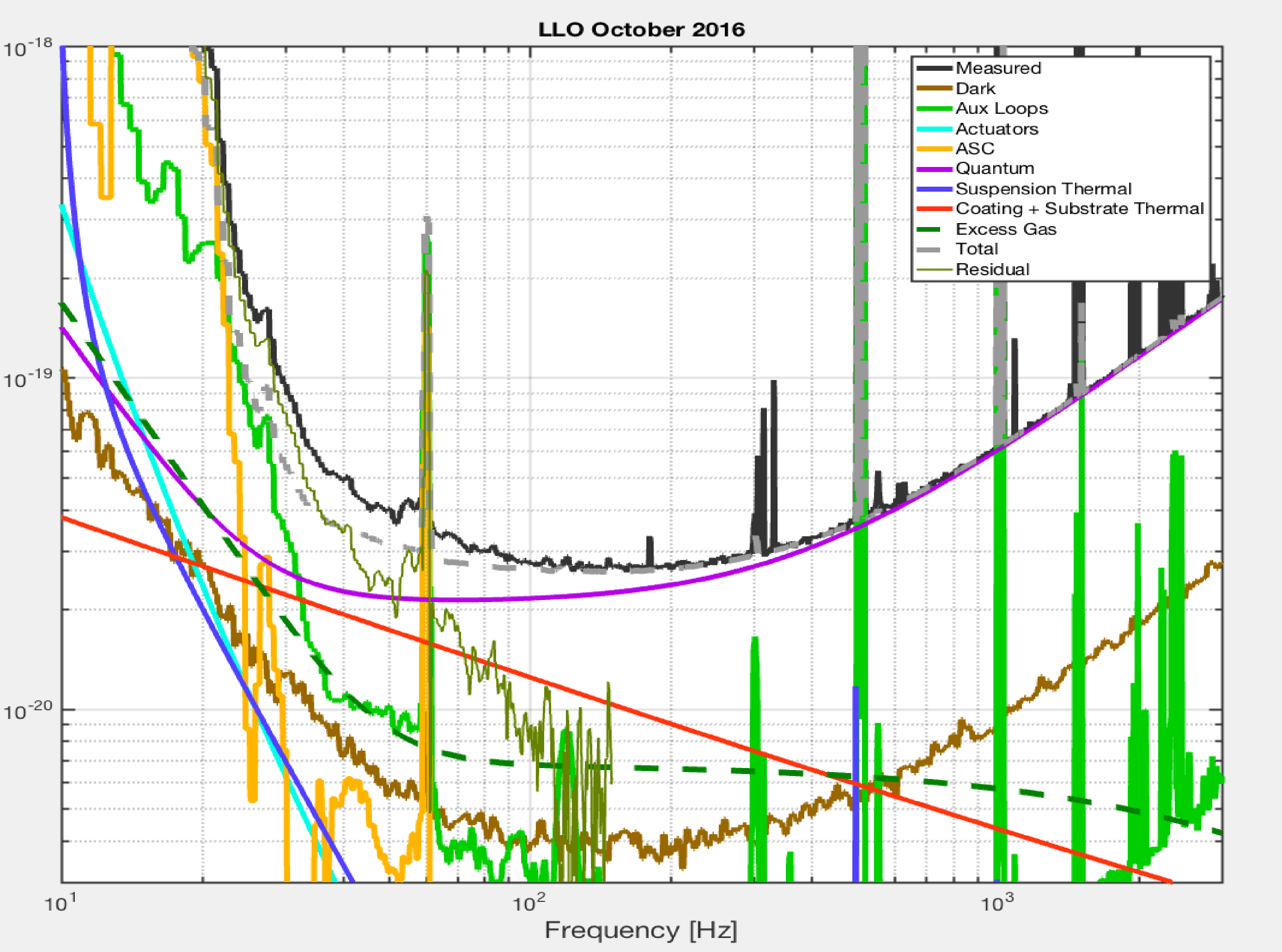
LLO October 2016
10^{-18}
10^{-19}
10^{-20}
10^{1}
10^{2}
10^{3}
Frequency [Hz]
Measured
Dark
Aux Loops
Actuators
ASC
Quantum
Suspension Thermal
Coating + Substrate Thermal
Excess Gas
Total
Residual

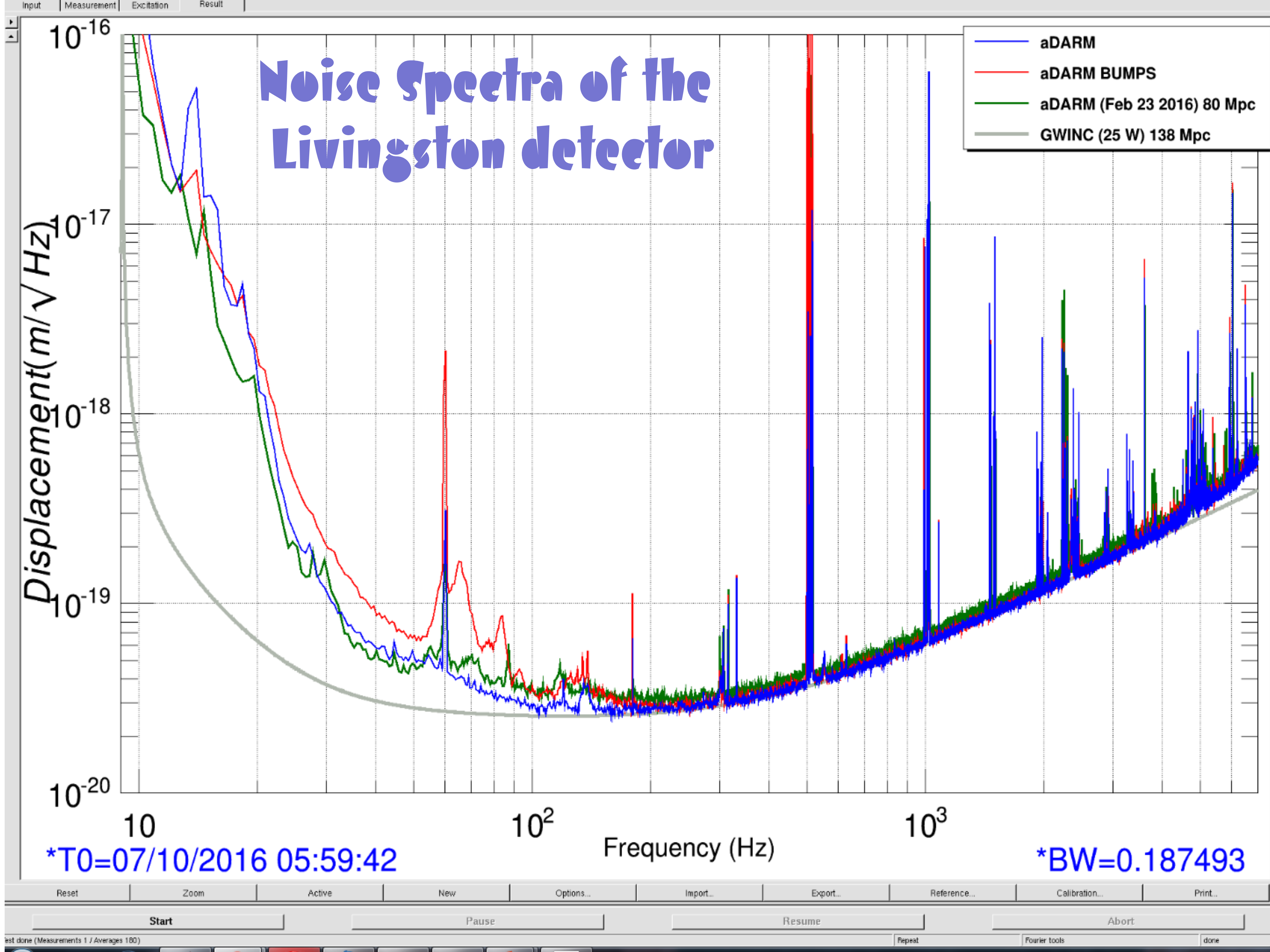
Input
Measurement
Excitation
Result
Noise Spectra of the
Livingston detector
aDARM
aDARM BUMPS
aDARM (Feb 23 2016) 80 Mpc
GWINC (25 W) 138 Mpc
Displacement(m/√Hz)
10^-16
10^-17
10^-18
10^-19
10^-20
10
10^2
10^3
Frequency (Hz)
*T0=07/10/2016 05:59:42
*BW=0.187493
Reset
Zoom
Active
New
Options...
Import...
Export...
Reference...
Calibration...
Print...
Start
Pause
Resume
Abort
est done (Measurements 1 / Averages 180)
Repeat
Fourier tools
done

Tests of General Relativity based on GW150914

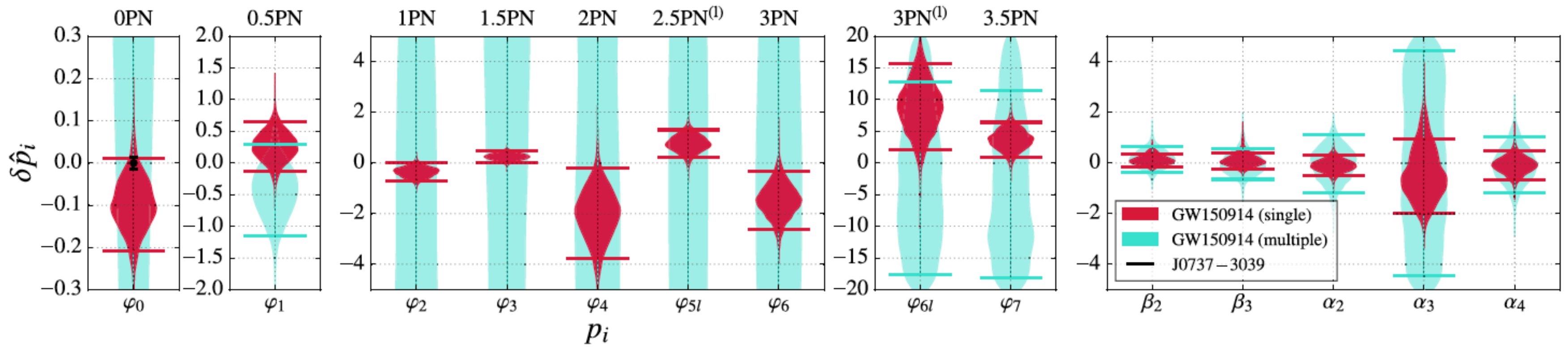

- Binary pulsar J0737-3039 results constrain only the 0PN term in a parameterized model of deviations from GR
- The dynamical evolution of the waveform through merger of GW150914 provides bounds on values to 3.5PN due to the dynamics of the merger
- Evolution of phase over time of the signal limits the amount of dispersion the signals suffered in propagating ~ 1.2 x 10^9 years
  - Lower limit on graviton \wavelength: $\lambda_g > 10^{13}$ km
  - Upper limit on graviton mass: $m_g \leq 1.2 \times 10^{-22}$ eV/c^2

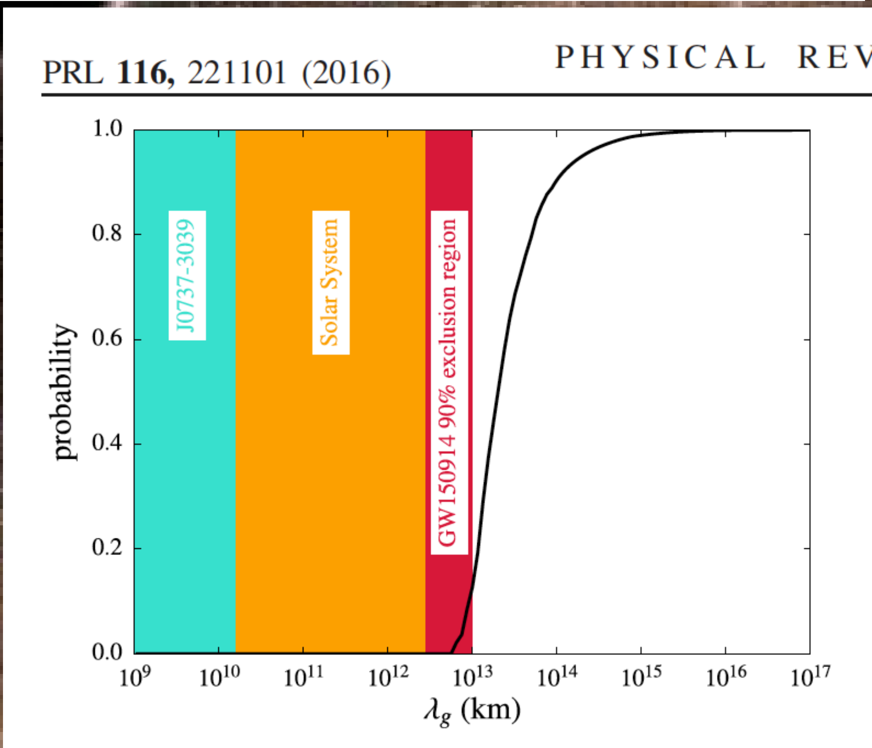

Parameter estimates for the 3 events

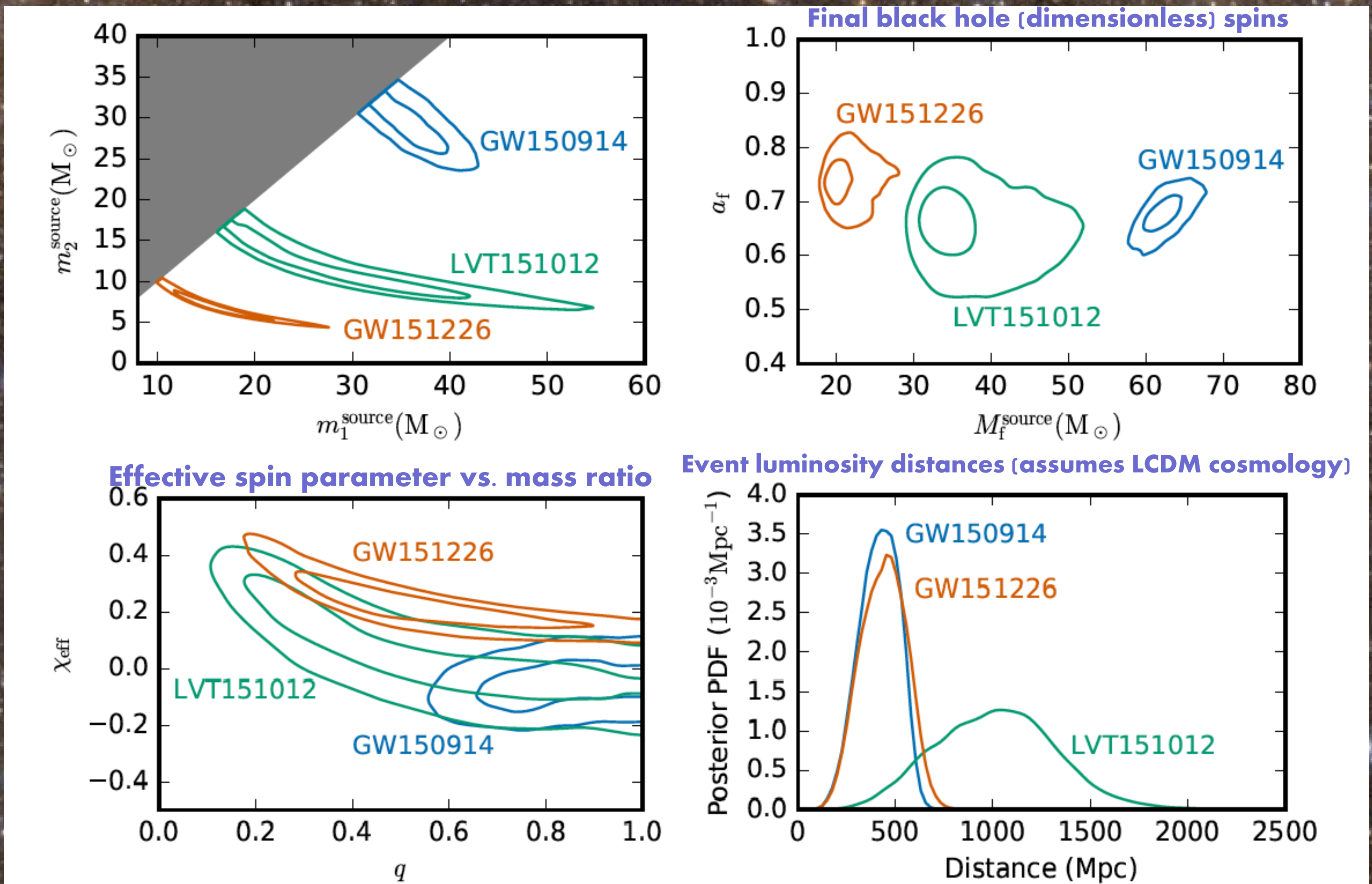

FIG. 4. Posterior probability densities of the masses, spins and distance to the three events GW150914, LVT151012 and GW151226. For the two dimensional distributions, the contours show 50% and 90% credible regions. *Top left:* component masses $m_1^{\rm source}$ and $m_2^{\rm source}$ for the three events. We use the convention that $m_1^{\rm source} \geq m_2^{\rm source}$, which produces the sharp cut in the two-dimensional distribution. For GW151226 and LVT151012, the contours follow lines of constant chirp mass ($\mathscr{M}^{\rm source} = 8.9^{+0.3}_{-0.3}\,M_\odot$ and $\mathscr{M}^{\rm source} = 15.1^{+1.4}_{-1.1}\,M_\odot$ respectively). In all three cases, both masses are consistent with being black holes. *Top right:* The mass and dimensionless spin magnitude of the final black holes. *Bottom left:* The effective spin and mass ratios of the binary components. *Bottom right:* The luminosity distance to the three events.

LIGO observations have bounded event rates for similar systems to those observed

- Rates within previously estimated values prior to detection
- Rates exclude most pessimistic values

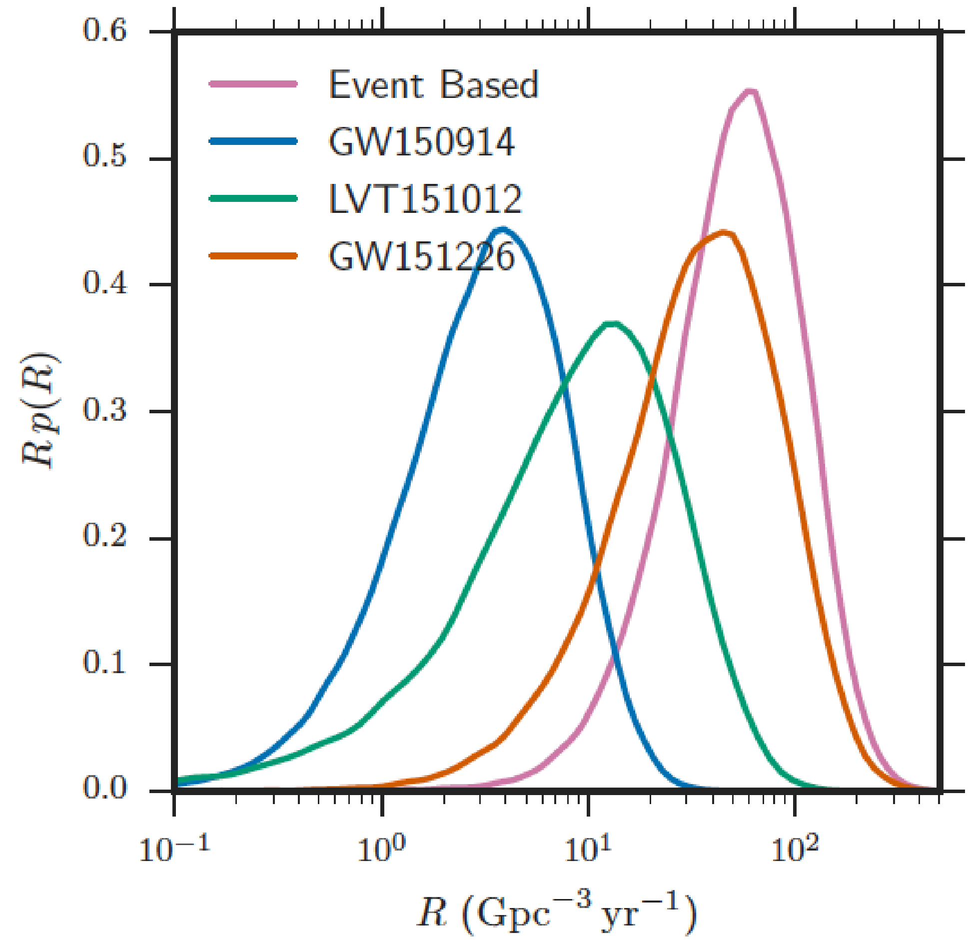

https://arxiv.org/abs/1606.04856

FIG. 9. The posterior density on the rate of GW150914-like BBH, LVT151012-like BBH, and GW151226-like BBH mergers. The event based rate is the sum of these. The median and 90% credible levels are given in Table II.

Observations cannot say much about spin at this time

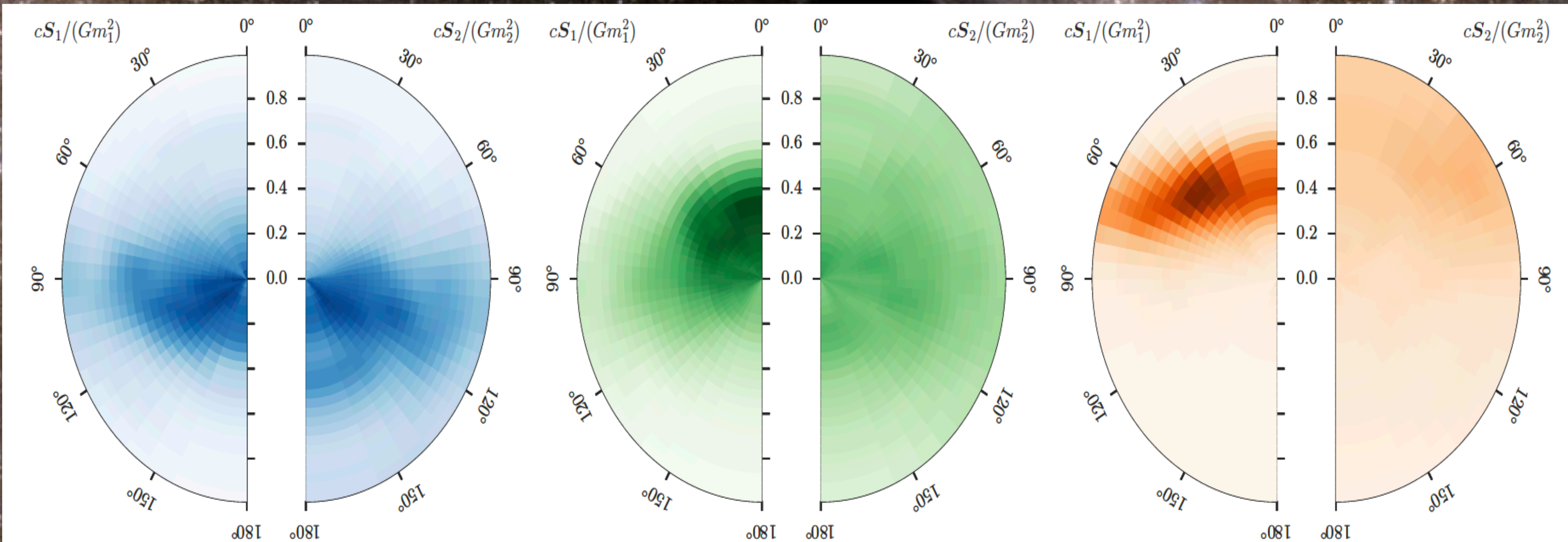

https://arxiv.org/abs/1606.04856

FIG. 5. Posterior probability distributions for for the dimensionless component spins $cS_1/(Gm_1^2)$ and $cS_2/(Gm_2^2)$ relative to the normal to the orbital plane L, marginalized over the azimuthal angles. The bins are constructed linearly in spin magnitude and the cosine of the tilt angles, and therefore have equal prior probability. The left plot shows the distribution for GW150914, the middle plot is for LVT151012 and the right plot is for GW151226.

TABLE IV. Parameters that characterise GW150914, GW151226 and LVT151012. For model parameters we report the median value with the range of the symmetric 90% credible interval [221]; we also quote selected 90% credible bounds. For the logarithm of the Bayes factor for a signal compared to Gaussian noise we report the mean and its 90% standard error from 4 parallel runs with a nested sampling algorithm [211], and for the deviance information criterion we report the mean and its 90% standard error from a Markov-chain Monte Carlo and a nested sampling run. The source redshift and source-frame masses assume standard cosmology [40]. Results are given for spin-aligned EOBNR and precessing IMRPhenom waveform models. The Overall results are computed by averaging the posteriors for the two models. For the Overall results we quote both the 90% credible interval or bound and an estimate for the 90% range of systematic error on this determined from the variance between waveform models. Further explanation of the parameters are given in [38].

	GW150914			GW151226			LVT151012		
	EOBNR	IMRPhenom	Overall	EOBNR	IMRPhenom	Overall	EOBNR	IMRPhenom	Overall
Detector frame									
Total mass $M/\mathrm{M}_\odot$	$71.0^{+4.6}_{-4.0}$	$71.2^{+3.5}_{-3.2}$	$71.1^{+4.1\pm0.7}_{-3.6\pm0.8}$	$23.6^{+8.0}_{-1.3}$	$23.8^{+5.1}_{-1.5}$	$23.7^{+6.5\pm2.2}_{-1.4\pm0.1}$	45^{+17}_{-4}	44^{+12}_{-3}	$44^{+16\pm5}_{-3\pm0}$
Chirp mass $\mathscr{M}/\mathrm{M}_\odot$	$30.4^{+2.3}_{-1.6}$	$30.7^{+1.5}_{-1.5}$	$30.6^{+1.9\pm0.3}_{-1.6\pm0.4}$	$9.71^{+0.08}_{-0.07}$	$9.72^{+0.06}_{-0.06}$	$9.72^{+0.07\pm0.01}_{-0.06\pm0.01}$	$18.1^{+1.3}_{-0.9}$	$18.1^{+0.8}_{-0.8}$	$18.1^{+1.0\pm0.5}_{-0.8\pm0.1}$
Primary mass $m_1/\mathrm{M}_\odot$	$40.2^{+5.2}_{-4.8}$	$38.5^{+5.4}_{-3.3}$	$39.4^{+5.4\pm1.3}_{-4.1\pm0.2}$	$15.3^{+10.8}_{-3.8}$	$15.8^{+7.2}_{-4.0}$	$15.6^{+9.0\pm2.6}_{-4.0\pm0.2}$	29^{+23}_{-8}	27^{+19}_{-6}	$28^{+21\pm5}_{-7\pm0}$
Secondary mass $m_2/\mathrm{M}_\odot$	$30.6^{+5.1}_{-4.2}$	$32.7^{+3.1}_{-4.9}$	$31.7^{+4.0\pm0.1}_{-4.9\pm1.2}$	$8.3^{+2.5}_{-2.9}$	$8.1^{+2.5}_{-2.1}$	$8.2^{+2.6\pm0.2}_{-2.5\pm0.5}$	15^{+5}_{-6}	16^{+4}_{-6}	$16^{+5\pm0}_{-6\pm1}$
Final mass $M_\mathrm{f}/\mathrm{M}_\odot$	$67.8^{+4.0}_{-3.6}$	$67.9^{+3.2}_{-2.9}$	$67.8^{+3.7\pm0.6}_{-3.3\pm0.7}$	$22.5^{+8.2}_{-1.4}$	$22.8^{+5.3}_{-1.6}$	$22.6^{+6.7\pm2.2}_{-1.5\pm0.1}$	43^{+17}_{-4}	42^{+13}_{-2}	$42^{+16\pm5}_{-3\pm0}$
Source frame									
Total mass $M^\mathrm{source}/\mathrm{M}_\odot$	$65.5^{+4.4}_{-3.9}$	$65.1^{+3.6}_{-3.1}$	$65.3^{+4.1\pm1.0}_{-3.4\pm0.3}$	$21.6^{+7.4}_{-1.6}$	$21.9^{+4.7}_{-1.7}$	$21.8^{+5.9\pm2.0}_{-1.7\pm0.1}$	38^{+15}_{-5}	37^{+11}_{-4}	$37^{+13\pm4}_{-4\pm0}$
Chirp mass $\mathscr{M}^\mathrm{source}/\mathrm{M}_\odot$	$28.1^{+2.1}_{-1.6}$	$28.1^{+1.6}_{-1.4}$	$28.1^{+1.8\pm0.4}_{-1.5\pm0.2}$	$8.87^{+0.35}_{-0.28}$	$8.90^{+0.31}_{-0.27}$	$8.88^{+0.33\pm0.01}_{-0.28\pm0.04}$	$15.2^{+1.5}_{-1.1}$	$15.0^{+1.3}_{-1.0}$	$15.1^{+1.4\pm0.3}_{-1.1\pm0.0}$
Primary mass $m_1^\mathrm{source}/\mathrm{M}_\odot$	$37.0^{+4.9}_{-4.4}$	$35.3^{+5.1}_{-3.1}$	$36.2^{+5.2\pm1.4}_{-3.8\pm0.4}$	$14.0^{+10.0}_{-3.5}$	$14.5^{+6.6}_{-3.7}$	$14.2^{+8.3\pm2.4}_{-3.7\pm0.2}$	24^{+19}_{-7}	23^{+16}_{-5}	$23^{+18\pm5}_{-6\pm0}$
Secondary mass $m_2^\mathrm{source}/\mathrm{M}_\odot$	$28.3^{+4.6}_{-3.9}$	$29.9^{+3.0}_{-4.5}$	$29.1^{+3.7\pm0.0}_{-4.4\pm0.9}$	$7.5^{+2.3}_{-2.6}$	$7.4^{+2.3}_{-2.0}$	$7.5^{+2.3\pm0.2}_{-2.3\pm0.4}$	13^{+4}_{-5}	14^{+4}_{-5}	$13^{+4\pm0}_{-5\pm0}$
Final mass $M_\mathrm{f}^\mathrm{source}/\mathrm{M}_\odot$	$62.5^{+3.9}_{-3.5}$	$62.1^{+3.3}_{-2.8}$	$62.3^{+3.7\pm0.9}_{-3.1\pm0.2}$	$20.6^{+7.6}_{-1.6}$	$20.9^{+4.8}_{-1.8}$	$20.8^{+6.1\pm2.0}_{-1.7\pm0.1}$	36^{+15}_{-4}	35^{+11}_{-3}	$35^{+14\pm4}_{-4\pm0}$
Energy radiated $E_\mathrm{rad}/(\mathrm{M}_\odot c^2)$	$2.98^{+0.55}_{-0.40}$	$3.02^{+0.36}_{-0.36}$	$3.00^{+0.47\pm0.13}_{-0.39\pm0.07}$	$1.02^{+0.09}_{-0.24}$	$0.99^{+0.11}_{-0.17}$	$1.00^{+0.10\pm0.01}_{-0.20\pm0.03}$	$1.48^{+0.39}_{-0.41}$	$1.51^{+0.29}_{-0.44}$	$1.50^{+0.33\pm0.05}_{-0.43\pm0.01}$
Mass ratio q	$0.77^{+0.20}_{-0.18}$	$0.85^{+0.13}_{-0.21}$	$0.81^{+0.17\pm0.02}_{-0.20\pm0.04}$	$0.54^{+0.40}_{-0.33}$	$0.51^{+0.39}_{-0.25}$	$0.52^{+0.40\pm0.03}_{-0.29\pm0.04}$	$0.53^{+0.42}_{-0.34}$	$0.60^{+0.35}_{-0.37}$	$0.57^{+0.38\pm0.01}_{-0.37\pm0.04}$
Effective inspiral spin χ_eff	$-0.08^{+0.17}_{-0.14}$	$-0.05^{+0.11}_{-0.12}$	$-0.06^{+0.14\pm0.02}_{-0.14\pm0.04}$	$0.21^{+0.24}_{-0.11}$	$0.22^{+0.15}_{-0.08}$	$0.21^{+0.20\pm0.07}_{-0.10\pm0.03}$	$0.06^{+0.31}_{-0.24}$	$0.01^{+0.26}_{-0.17}$	$0.03^{+0.31\pm0.08}_{-0.20\pm0.02}$
Primary spin magnitude a_1	$0.33^{+0.39}_{-0.29}$	$0.30^{+0.54}_{-0.27}$	$0.32^{+0.47\pm0.10}_{-0.29\pm0.01}$	$0.42^{+0.35}_{-0.37}$	$0.55^{+0.35}_{-0.42}$	$0.49^{+0.37\pm0.11}_{-0.42\pm0.07}$	$0.31^{+0.46}_{-0.27}$	$0.31^{+0.50}_{-0.28}$	$0.31^{+0.48\pm0.03}_{-0.28\pm0.00}$
Secondary spin magnitude a_2	$0.62^{+0.35}_{-0.54}$	$0.36^{+0.53}_{-0.33}$	$0.48^{+0.47\pm0.08}_{-0.43\pm0.03}$	$0.51^{+0.44}_{-0.46}$	$0.52^{+0.42}_{-0.47}$	$0.52^{+0.43\pm0.01}_{-0.47\pm0.00}$	$0.49^{+0.45}_{-0.44}$	$0.42^{+0.50}_{-0.38}$	$0.45^{+0.48\pm0.02}_{-0.41\pm0.01}$
Final spin a_f	$0.68^{+0.05}_{-0.07}$	$0.68^{+0.06}_{-0.05}$	$0.68^{+0.05\pm0.01}_{-0.06\pm0.02}$	$0.73^{+0.05}_{-0.06}$	$0.75^{+0.07}_{-0.05}$	$0.74^{+0.06\pm0.03}_{-0.06\pm0.03}$	$0.65^{+0.09}_{-0.10}$	$0.66^{+0.08}_{-0.10}$	$0.66^{+0.09\pm0.00}_{-0.10\pm0.02}$
Luminosity distance $D_\mathrm{L}/\mathrm{Mpc}$	400^{+160}_{-180}	440^{+140}_{-170}	$420^{+150\pm20}_{-180\pm40}$	450^{+180}_{-210}	440^{+170}_{-180}	$440^{+180\pm20}_{-190\pm10}$	1000^{+540}_{-490}	1030^{+480}_{-480}	$1020^{+500\pm20}_{-490\pm40}$
Source redshift z	$0.086^{+0.031}_{-0.036}$	$0.094^{+0.027}_{-0.034}$	$0.090^{+0.029\pm0.003}_{-0.036\pm0.008}$	$0.096^{+0.035}_{-0.042}$	$0.092^{+0.033}_{-0.037}$	$0.094^{+0.035\pm0.004}_{-0.039\pm0.001}$	$0.198^{+0.091}_{-0.092}$	$0.204^{+0.082}_{-0.088}$	$0.201^{+0.086\pm0.003}_{-0.091\pm0.008}$
Upper bound									
Primary spin magnitude a_1	0.62	0.73	0.67 ± 0.09	0.68	0.83	0.77 ± 0.12	0.64	0.69	0.67 ± 0.04
Secondary spin magnitude a_2	0.93	0.80	0.90 ± 0.12	0.90	0.89	0.90 ± 0.01	0.89	0.85	0.87 ± 0.04
Lower bound									
Mass ratio q	0.62	0.68	0.65 ± 0.05	0.25	0.30	0.28 ± 0.04	0.22	0.28	0.24 ± 0.05
Log Bayes factor $\ln\mathscr{B}_{\mathrm{s/n}}$	287.7 ± 0.1	289.8 ± 0.3	—	59.5 ± 0.1	60.2 ± 0.2	—	22.8 ± 0.2	23.0 ± 0.1	—
Information criterion DIC	32977.2 ± 0.3	32973.1 ± 0.1	—	34296.4 ± 0.2	34295.1 ± 0.1	—	94695.8 ± 0.0	94692.9 ± 0.0	—

Neutron Star Equation of State

- Neutron stars host the highest densities in the (visible) universe
- Measuring their equation of state requires joint measurement of radius and mass
- Possible with EM, but challenging
  - Mass estimates not always reliable
  - Radius estimates non often available and not always reliable
  - NICER to launch 2016, 5% precision

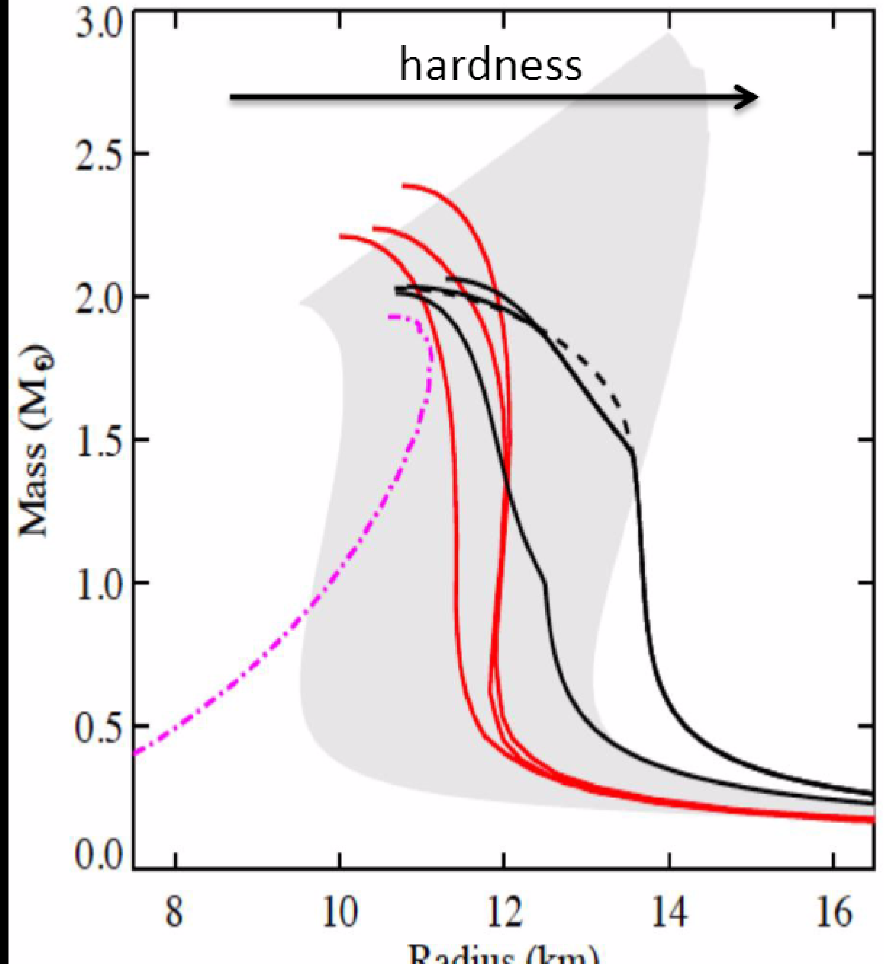

Watts+, 1602.01081

Neutron Star Equation of State

- In a CBC, each NS will feel the tidal field of the companion, which induces a quadrupole moment

$$Q_{ij} = - / \, (EOS, m) \, T_{ij}$$

- Known leading and next-to-leading effects on GW phasing
- Early studies considered single events, with contradictory findings (Read+ PRD 79 124033; Hinderer+ PRD 81 123016, many others)
- Markakis+ JPCS 189 012024 considered multiple events but used Fished matrix, unreliable at low signal-to-noise ratios (Vallisneri PRD 77 042001, Vitale+ PRD 84 104020)
- First fully Bayesian approach in 2013 (Del Pozzo+ PRL 11 071110)
- Also see Wade+, and many more.

GW – Electromagnetic connection

- CBC containing neutron stars are expected to be bright in the EM band
  - Progenitors of short GRBs?
  - Rich variety of frequencies and timescales
- Core collapse supernovae are believed to power long GRBs
- And are BBH luminous??

Metzger, Berger

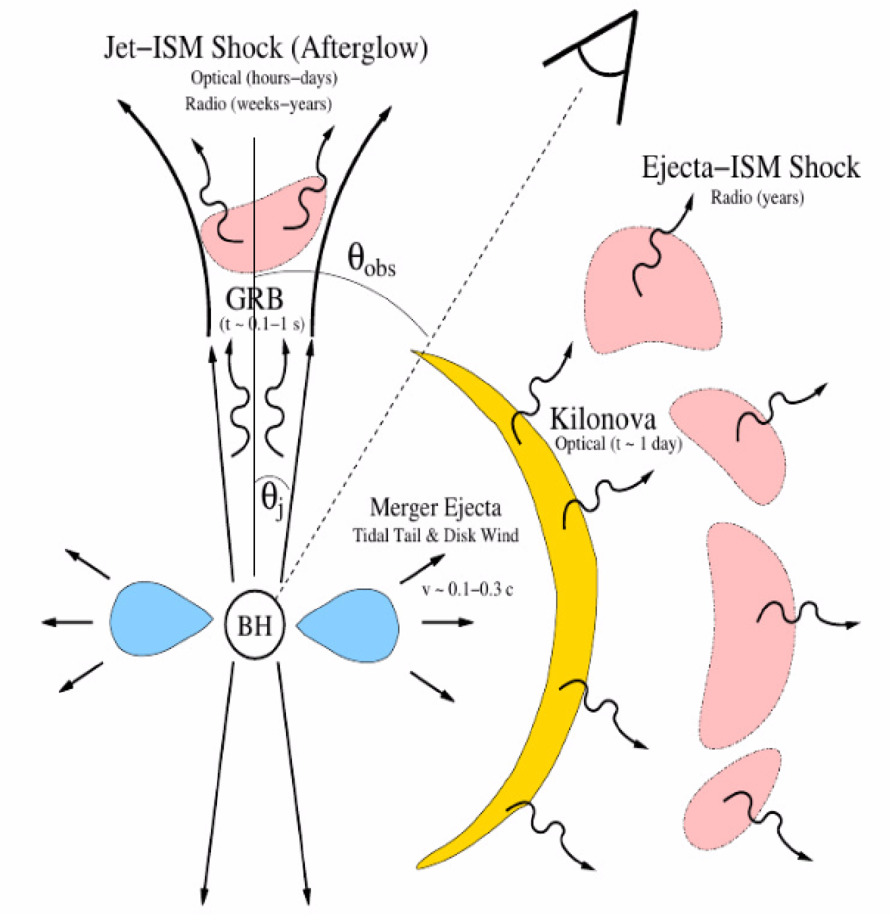

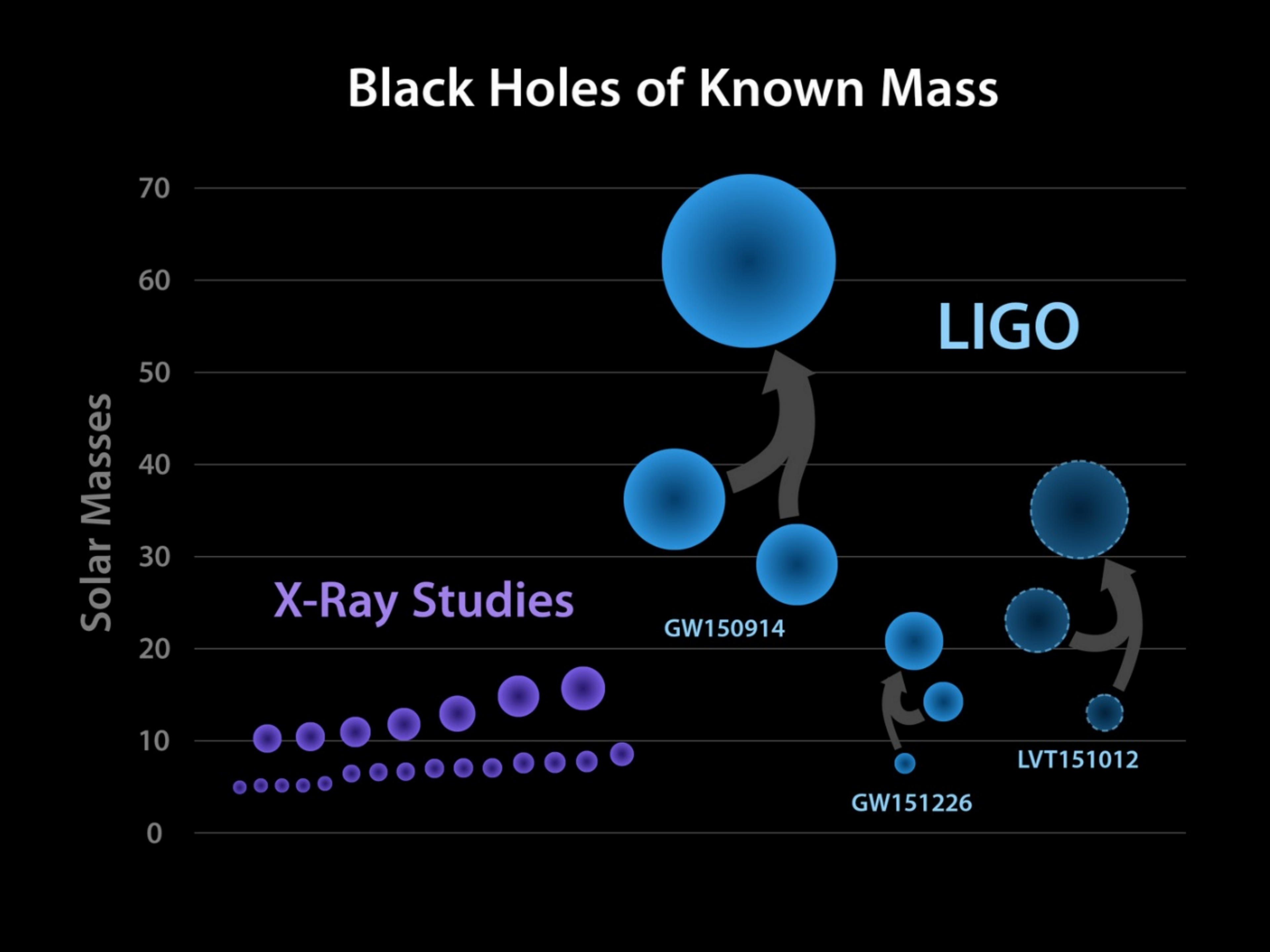

Black Holes of Known Mass
Solar Masses
70
60
50
40
30
20
10
0
X-Ray Studies
LIGO
GW150914
GW151226
LVT151012

CBC and their formation channels

- Measuring masses and spins can help determine channel and environment in which BH and CBC are formed
- Two main formation channels
  - Common envelope evolution
    - Galactic fields
    - Final masses not too different
    - Aligned spins
  - Dynamical capture
    - Globular clusters
    - Any mass ratio (?)
    - Misaligned spins

LIGO

Cosmography with GWs

- Gravitational waves provide direct measurement of *luminosity distance*
- If the *redshift* of the source can be estimated in some other way one can measure cosmological parameters.

$$D_L(z) = \begin{cases} \frac{(1+z)}{\sqrt{\Omega_k}} \sinh[\sqrt{\Omega_k} \int_0^z \frac{dz'}{H(z')}] & \text{for} \quad \Omega_k > 0 \\ (1+z) \int_0^z \frac{dz'}{H(z')} & \text{for} \quad \Omega_k = 0 \\ \frac{(1+z)}{\sqrt{|\Omega_k|}} \sin[\sqrt{|\Omega_k|} \int_0^z \frac{dz'}{H(z')}] & \text{for} \quad \Omega_k < 0 \end{cases}$$

$$H(z) = H_0 \sqrt{\Omega_m (1+z)^3 + \Omega_k (1+z)^2 + \Omega_\Lambda E(z, w(z))}$$

Gravitational Waves propagate through Space

SIMULATION OF THE BINARY BLACK-HOLE COALESCENCE GW150914

SIMULATION OF THE BINARY BLACK-HOLE COALESCENCE GW151226

Black Holes Everywhere

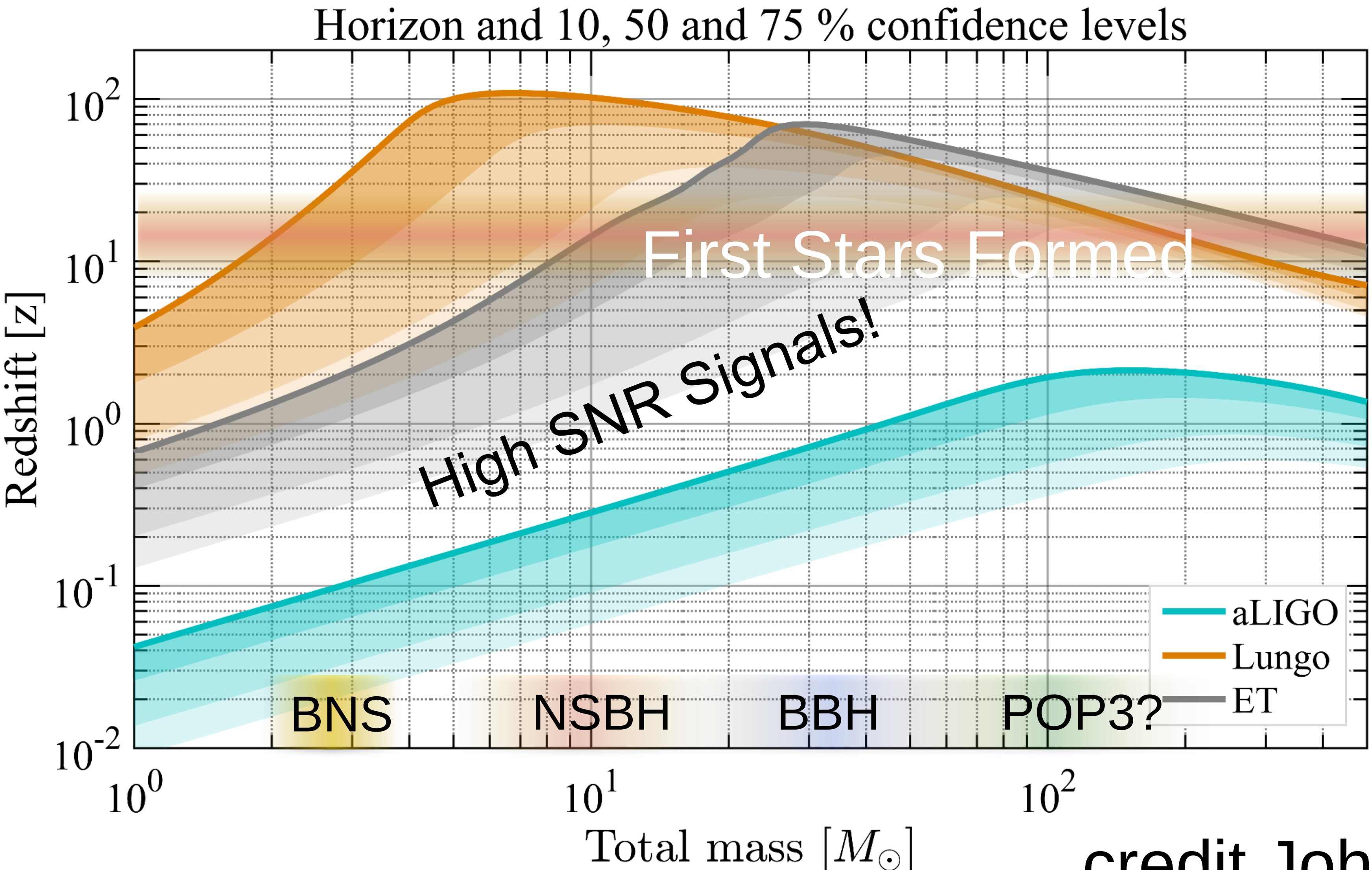

credit John M

Early Noise Progression Livingston 4km

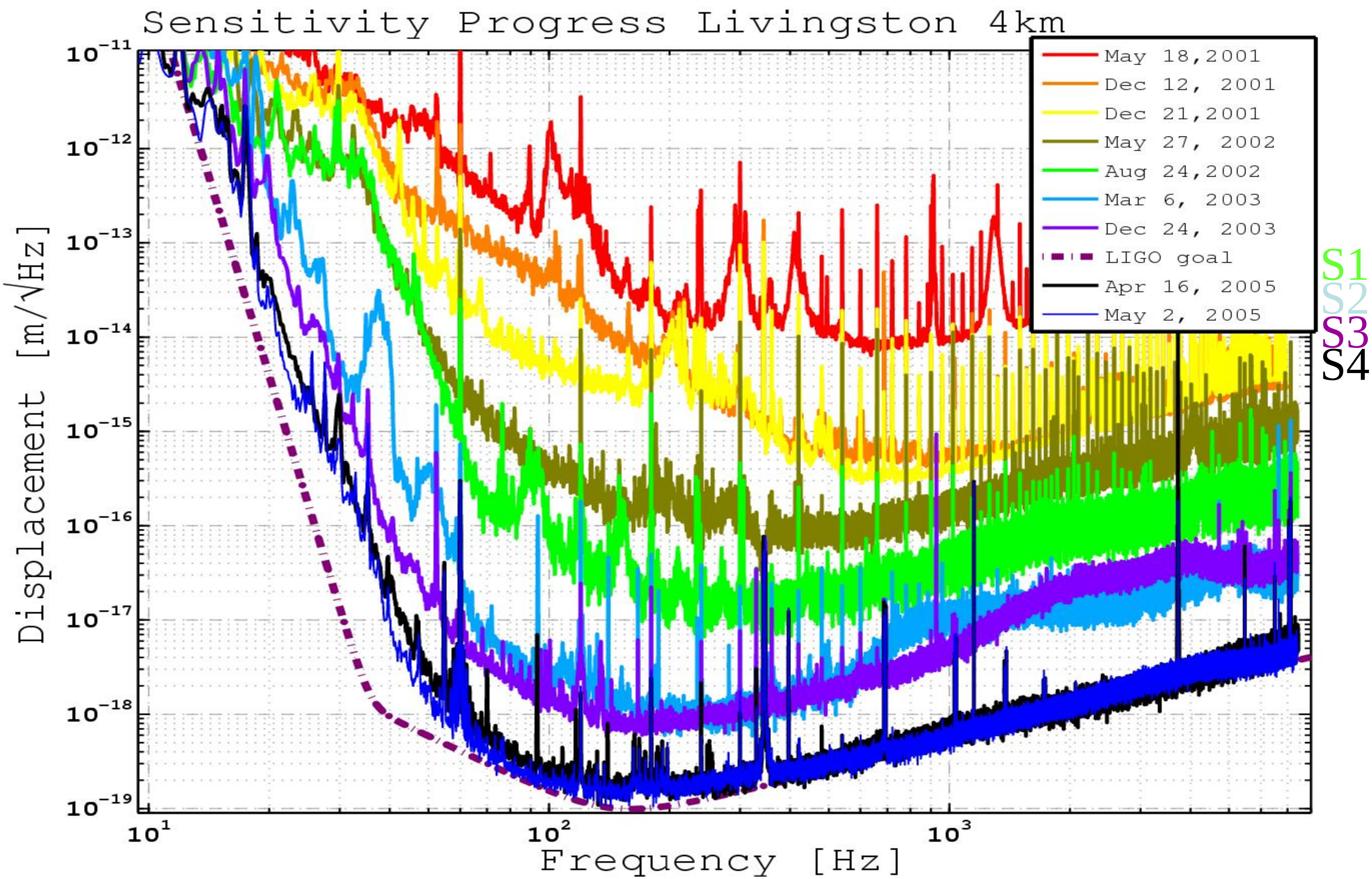

How to Beat the Quantum Limit

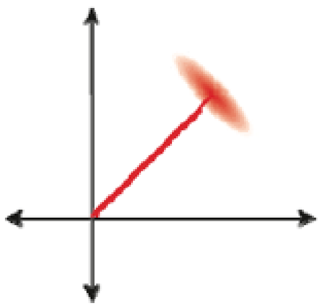

Reduced Amplitude Noise

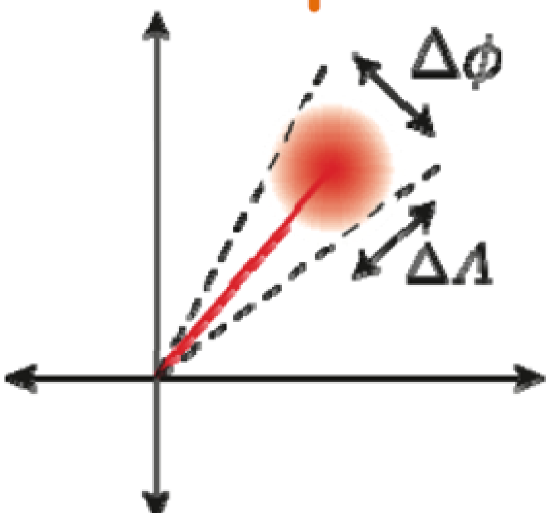

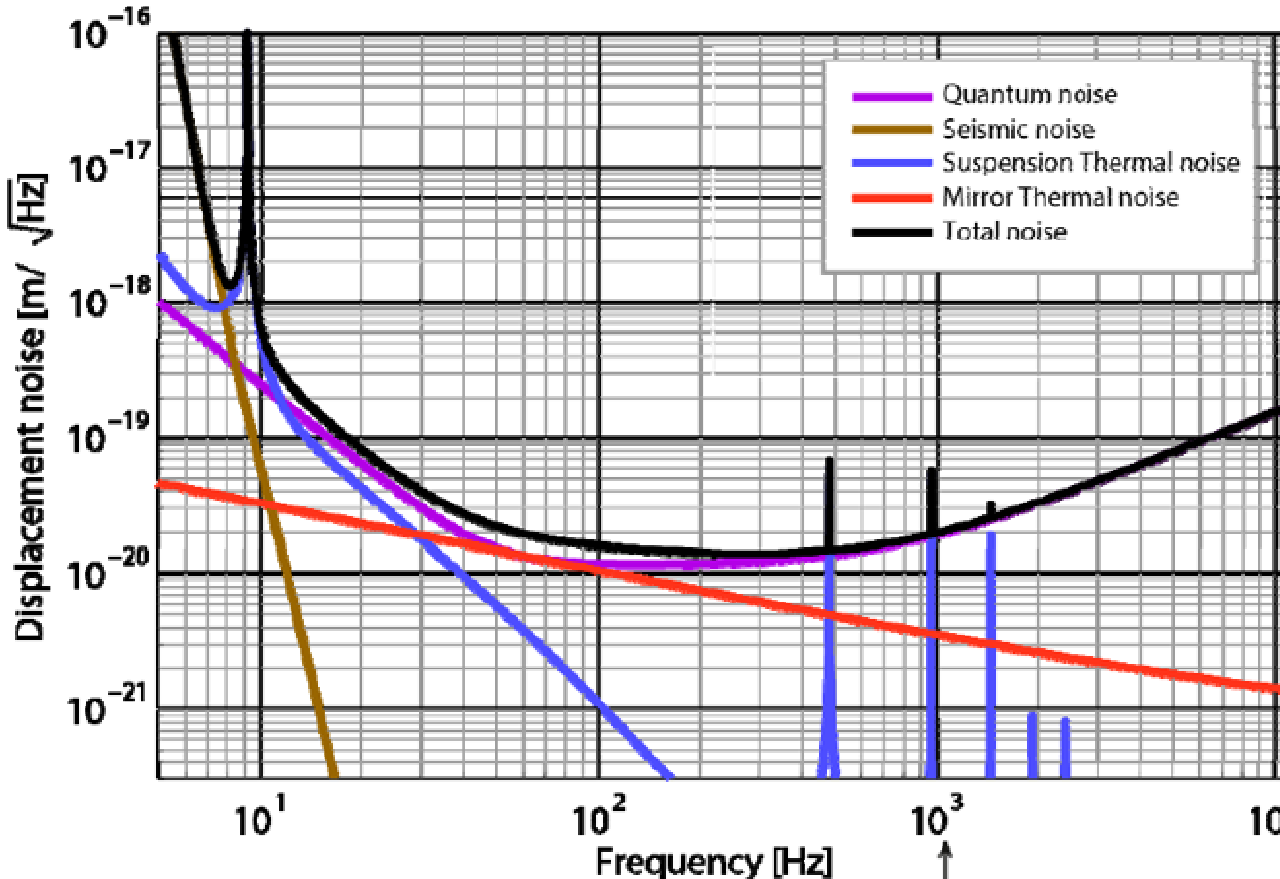

Reduced Phase Noise

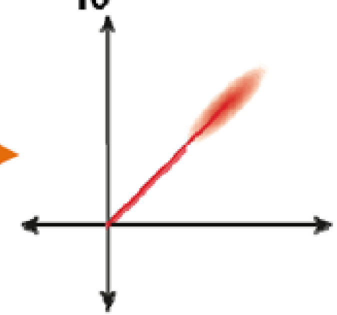

Observed Effects of Gravity's Distortion of Space

Gravitational Lensing – light bends around massive object

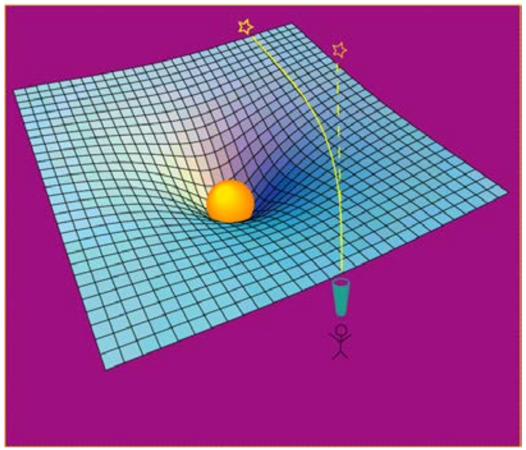

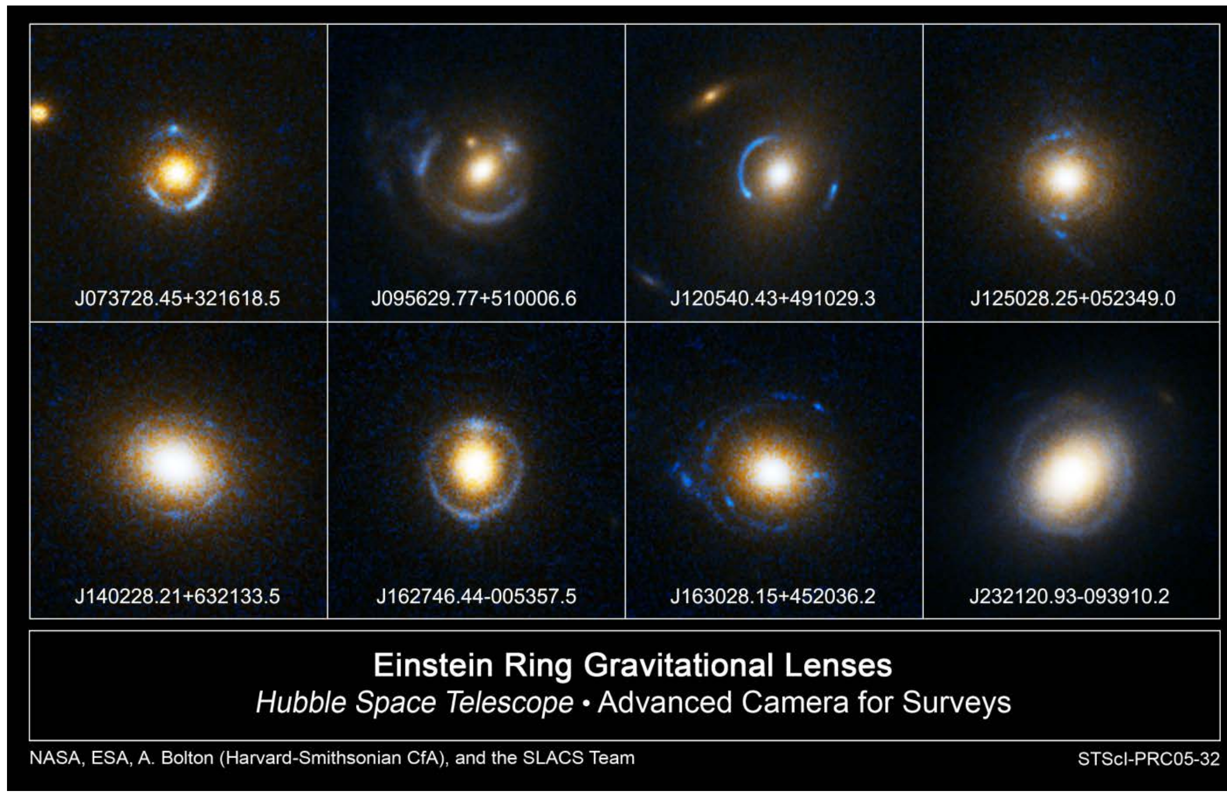

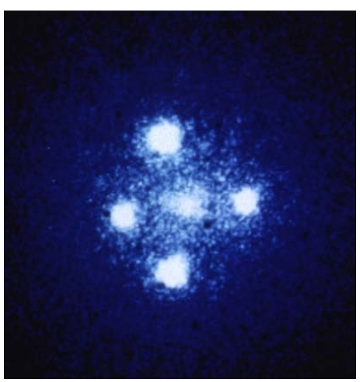

"Einstein's Cross" – quasar's light bends around a galaxy.

Seismic Noise

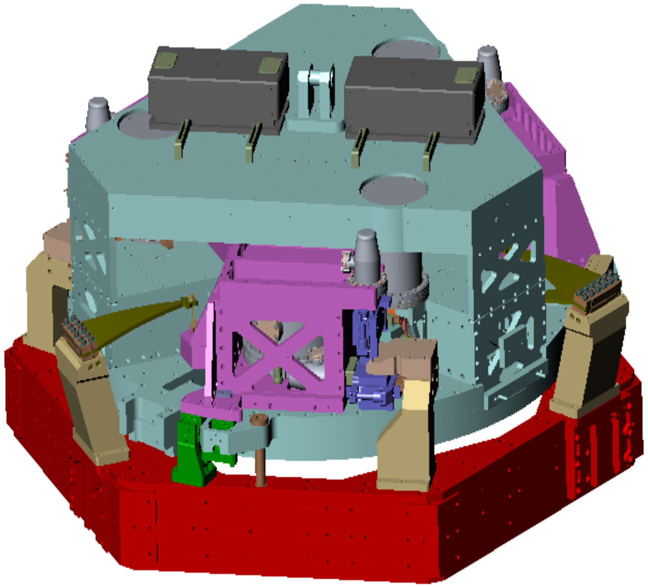

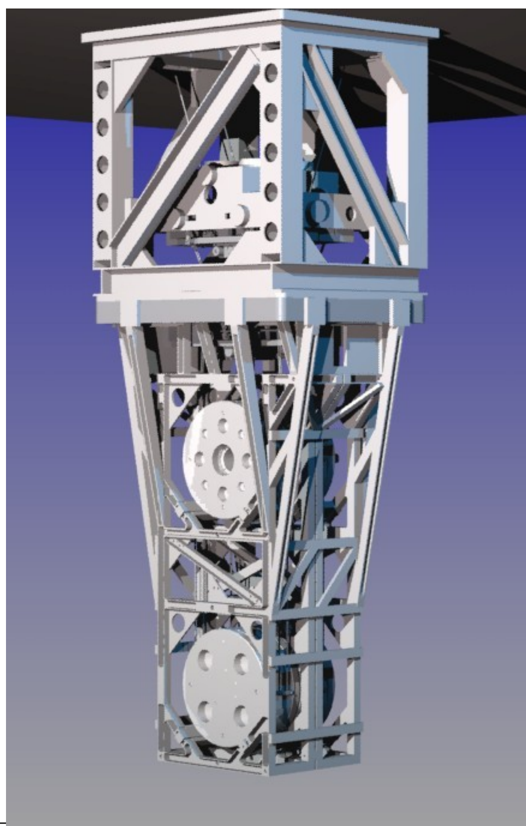

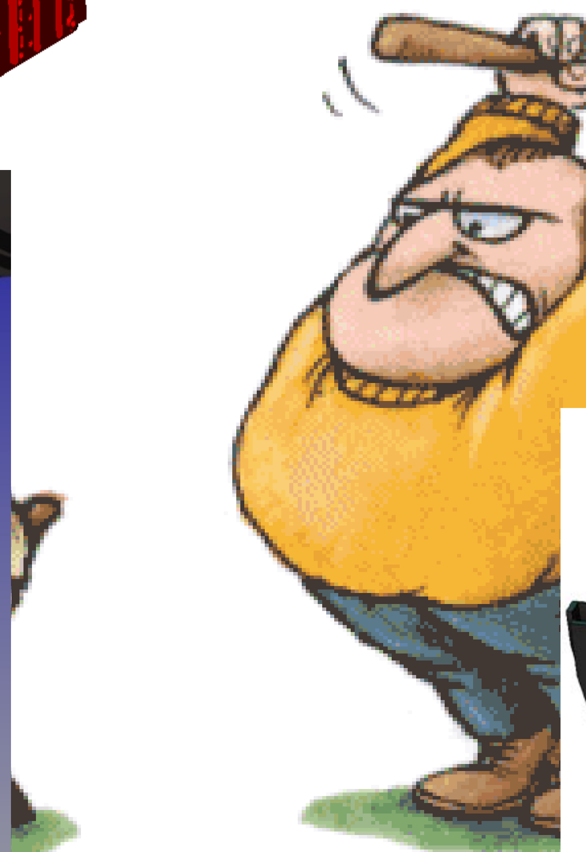

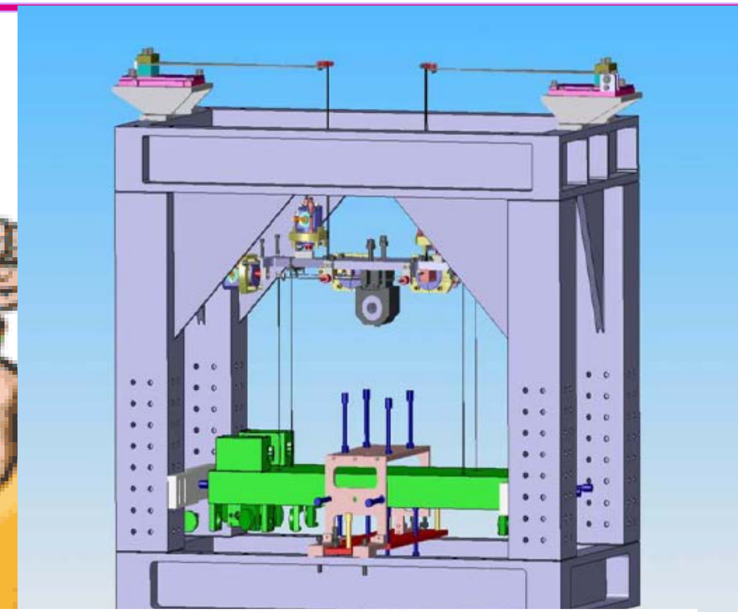

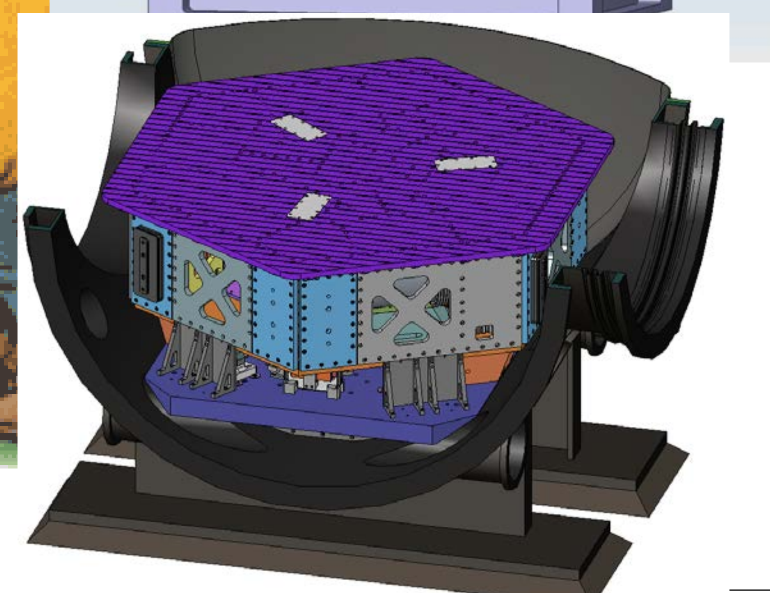

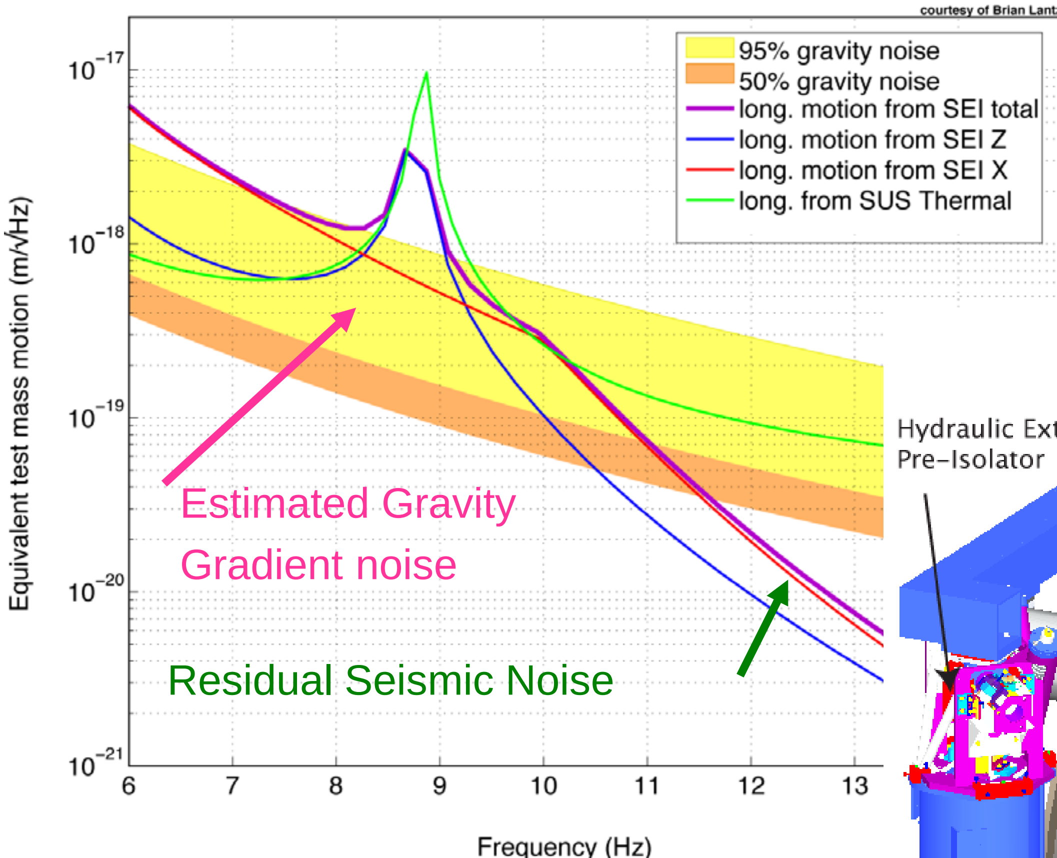

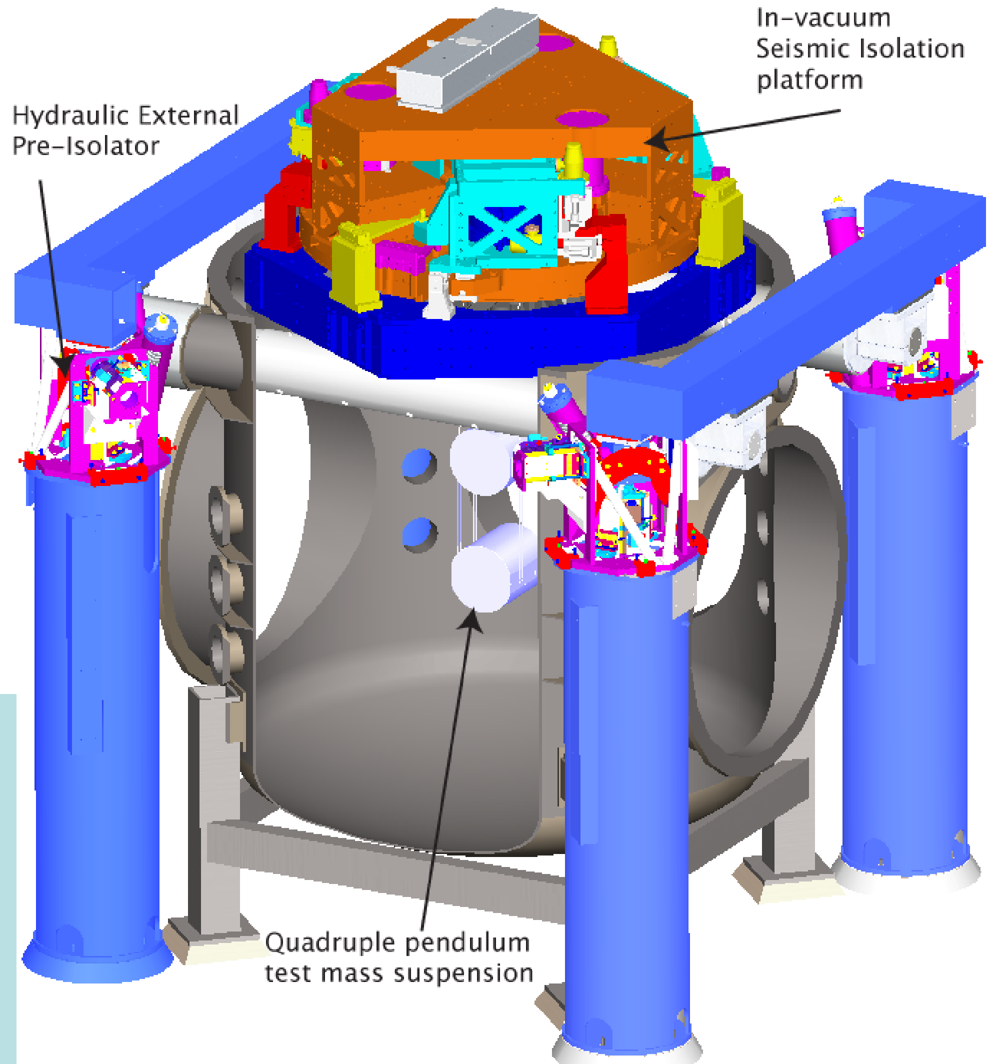

Advance Ligo Seismic Isolation is designed so as not to be a limiting noise source

Quad Suspensions

- Quadruple pendulum:
  - ~10^7 attenuation @10 Hz
  - Controls applied to upper layers; noise filtered from test masses

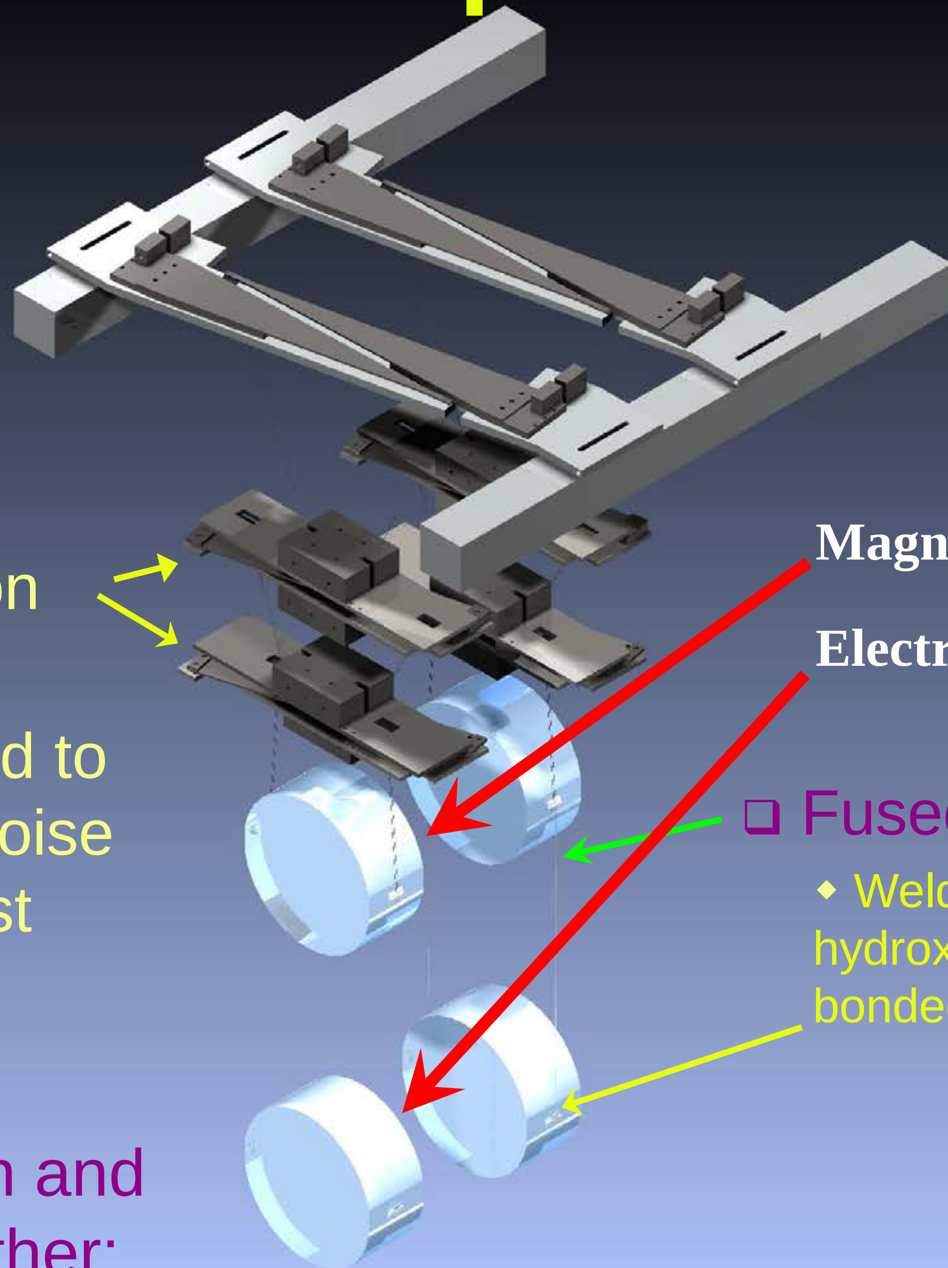

- Fused silica fiber
  - Welded to ‘ears’, hydroxy-catalysis bonded to optic

- Seismic isolation and suspension together:

New Internal Seismic Isolation System

Black Hole Mergers

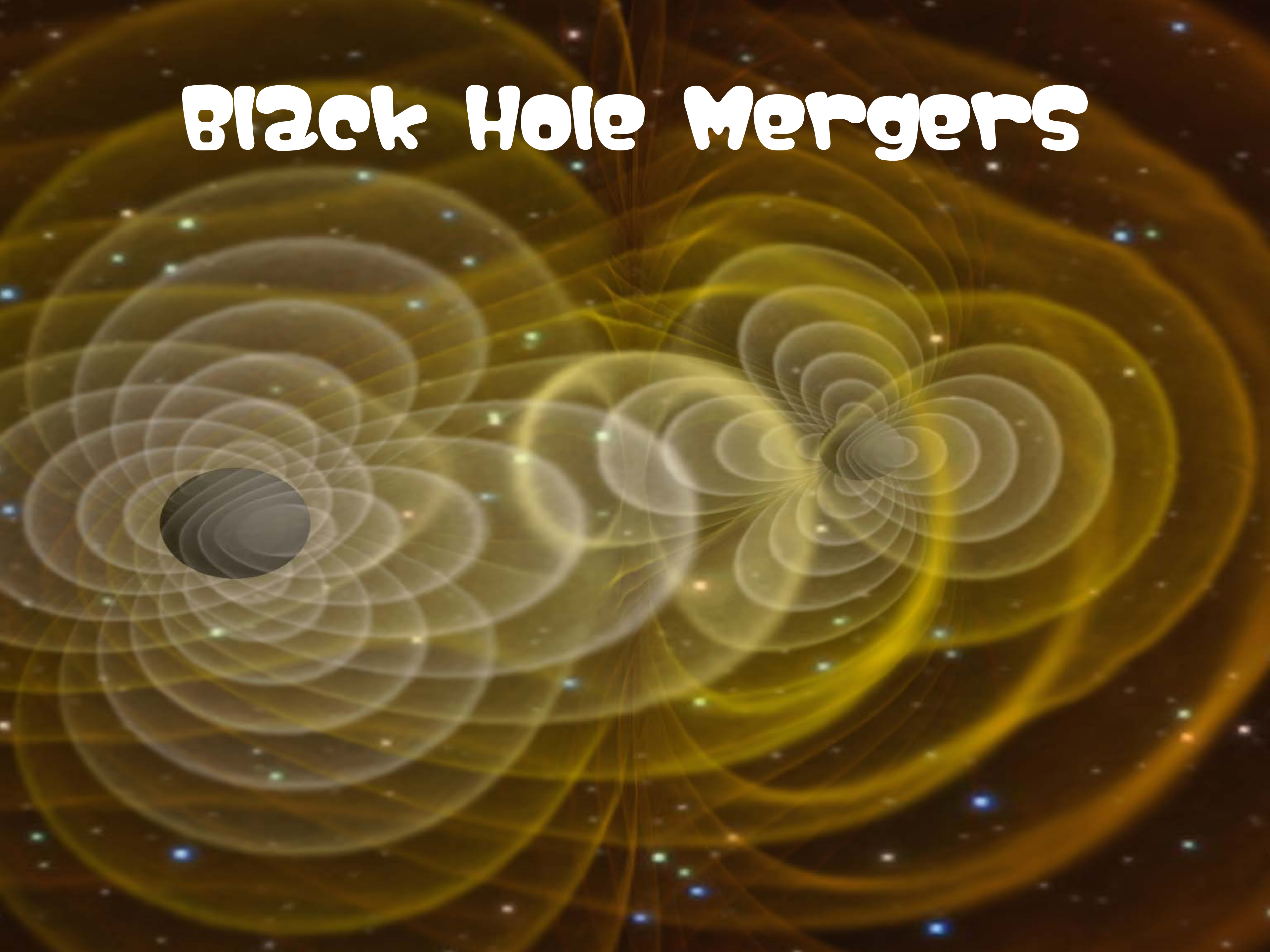

Stochastic Waves

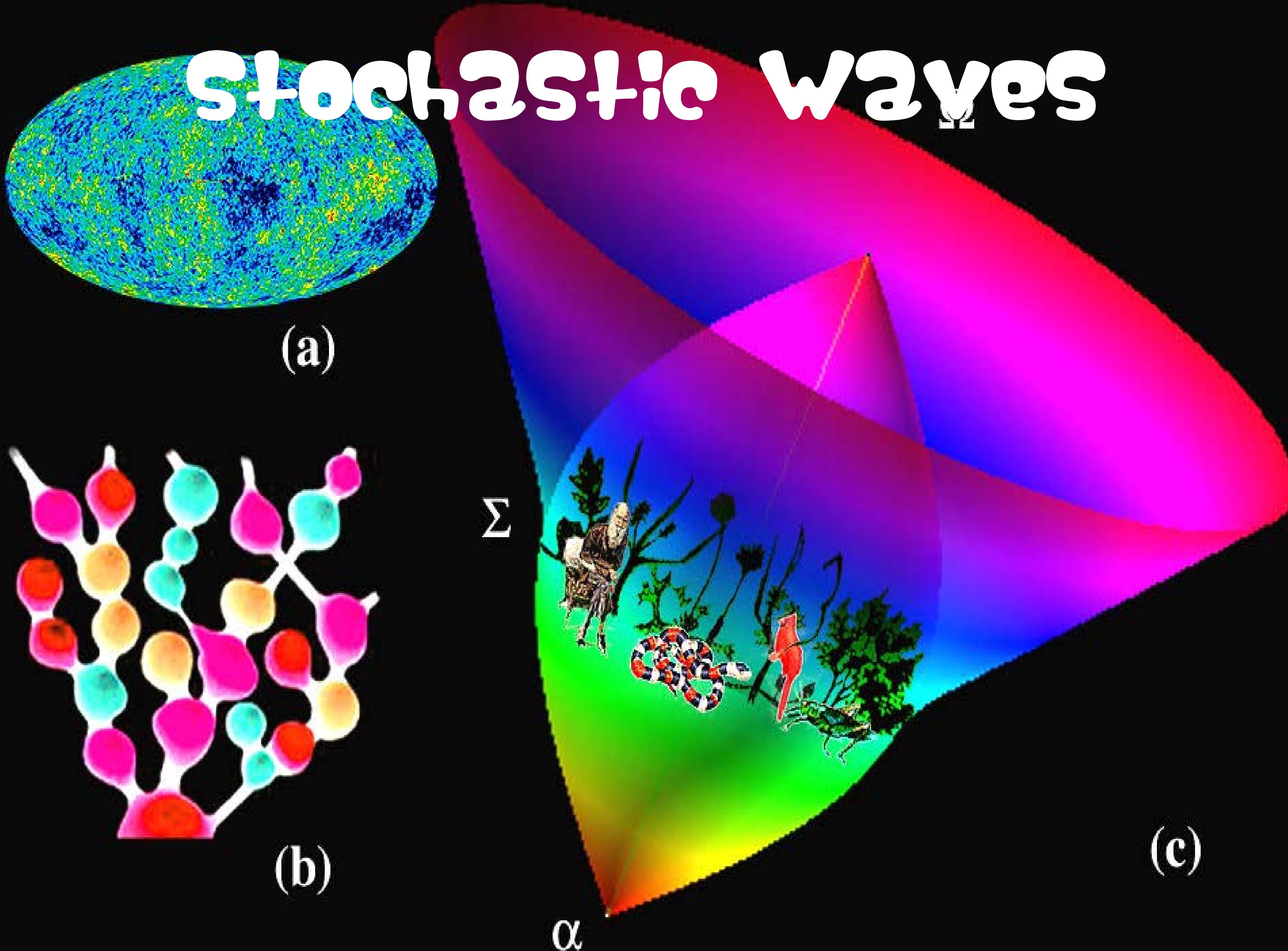

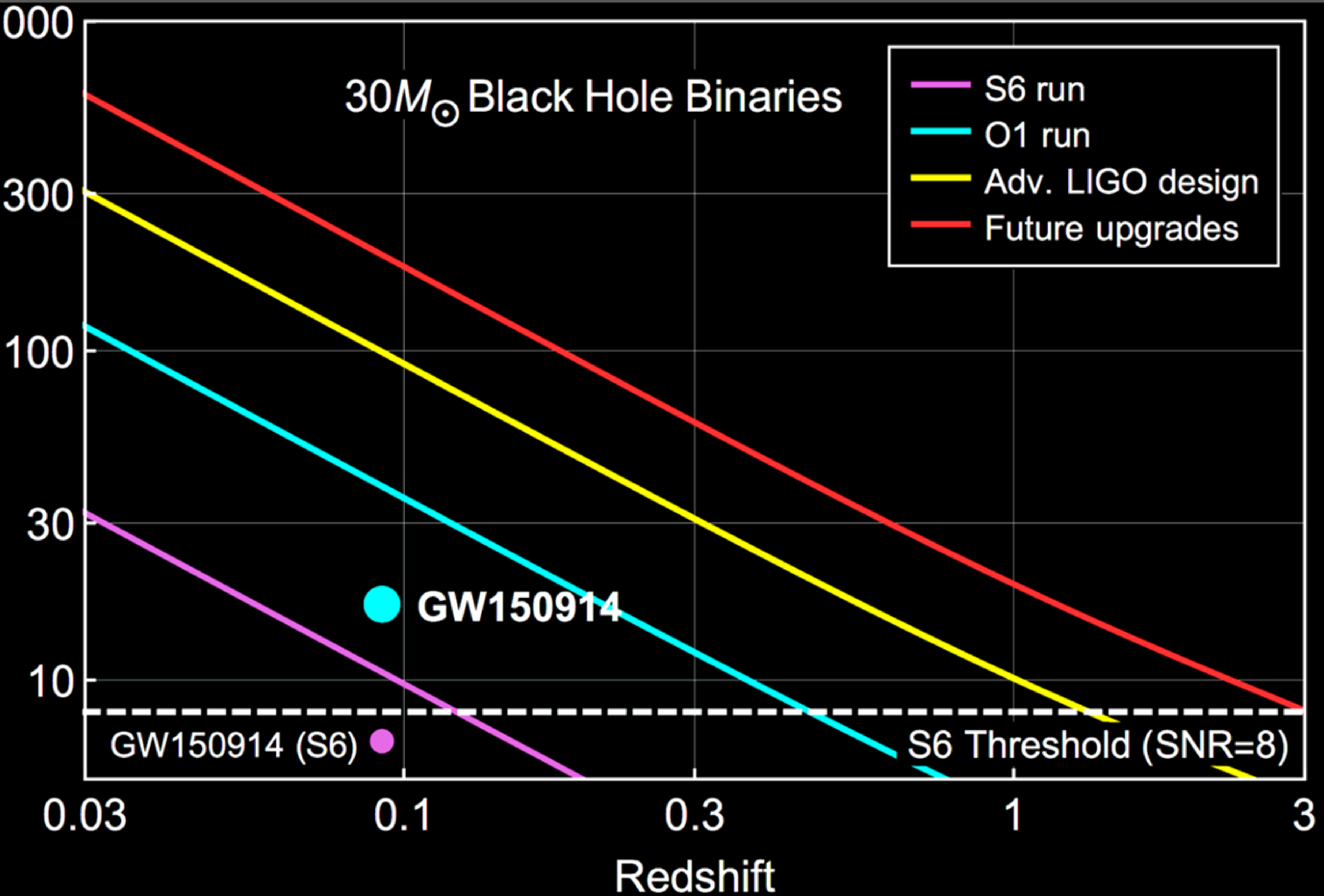

Abbott,... DAB, et al. Phys. Rev. Lett. **116**,

Bar Detectors

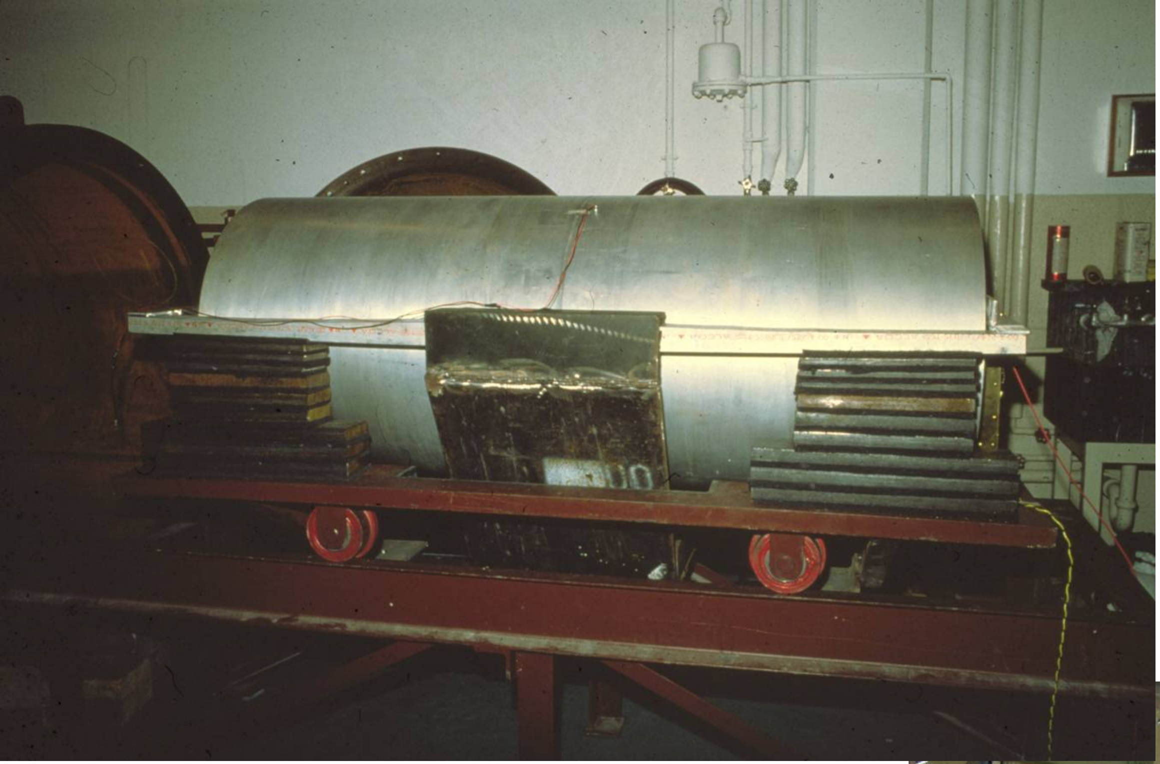

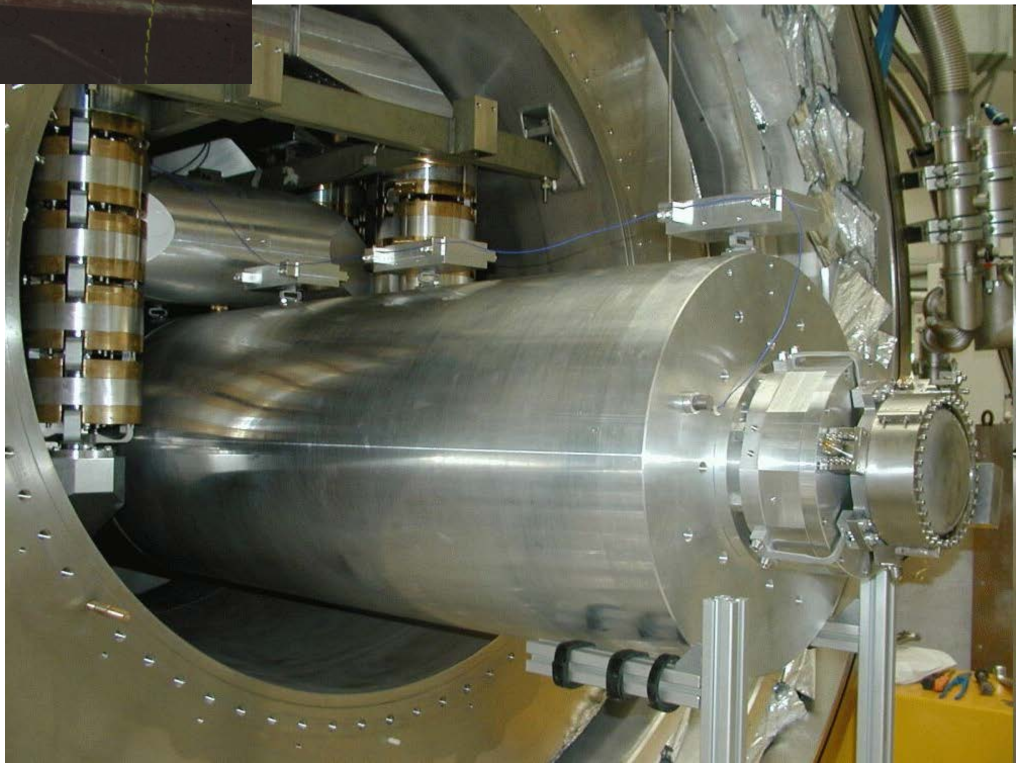

Vacuum tube enclosures test

Advanced Ligo